Cell Reports

Article

A delicate balance between antibody evasion and ACE2 affinity for Omicron BA.2.75

Graphical abstract

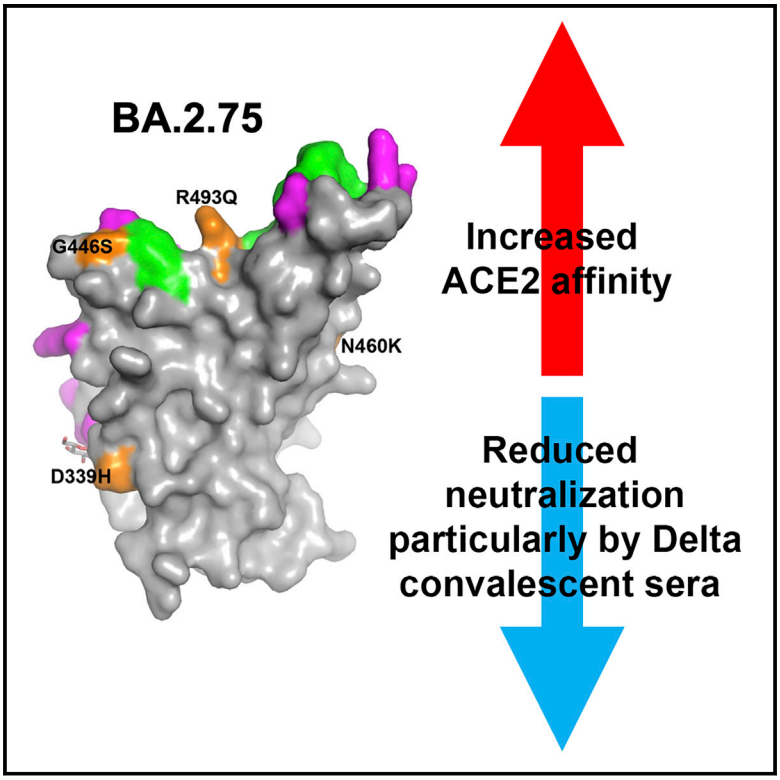

Highlights

- BA.2.75 affinity for ACE2 is increased 9-fold compared with BA.2
- N460K increases neutralization escape and likely increases ACE2 affinity
- The revertant R493Q decreases neutralization escape but increases ACE2 affinity
- Affinity to ACE2 appears to be prioritized over neutralization escape

Authors

Jiandong Huo, Aiste Dijokaite-Guraliuc, Chang Liu, ..., Jingshan Ren, David I. Stuart, Gavin R. Screaton

Correspondence

huojiandong@gird.cn (J.H.), liz@strubi.ox.ac.uk (E.E.F.), juthathip.mongkolsapaya@well.ox.ac.uk (J.M.), ren@strubi.ox.ac.uk (J.R.), dave@strubi.ox.ac.uk (D.I.S.), gavin.screaton@medsci.ox.ac.uk (G.R.S.)

In brief

Huo et al. characterize the SARS-CoV-2 variant BA.2.75 (originally identified in India). Its affinity for ACE2 is increased 9-fold over BA.2, and there is evidence of escape of BA.2.75 from immune serum, particularly from Delta infection. ACE2 affinity appears to be prioritized over greater escape via the R493Q reversion mutation.

Huo et al., 2023, Cell Reports *42*, 111903
January 31, 2023
https://doi.org/10.1016/j.celrep.2022.111903

CellPress

Cell Reports

CellPress
OPEN ACCESS

Article

A delicate balance between antibody evasion and ACE2 affinity for Omicron BA.2.75

Jiandong Huo,[1,2,3,20,*] Aiste Dijokaite-Guraliuc,[4,20] Chang Liu,[4,5,20] Daming Zhou,[2,5] Helen M. Ginn,[6] Raksha Das,[4] Piyada Supasa,[4] Muneeswaran Selvaraj,[4] Rungtiwa Nutalai,[4] Aekkachai Tuekprakhon,[4] Helen M.E. Duyvesteyn,[2] Alexander J. Mentzer,[4,7] Donal Skelly,[7,8,9] Thomas G. Ritter,[7] Ali Amini,[7,8,10] Sagida Bibi,[11] Sandra Adele,[7] Sile Ann Johnson,[7] Neil G. Paterson,[6] Mark A. Williams,[6] David R. Hall,[6] Megan Plowright,[12,13] Thomas A.H. Newman,[12,13] Hailey Hornsby,[12] Thushan I. de Silva,[12,13] Nigel Temperton,[14] Paul Klenerman,[7,8,10,15] Eleanor Barnes,[7,8,10,15] Susanna J. Dunachie,[7,8,16,17,18] Andrew J. Pollard,[11,15] Teresa Lambe,[5,11] Philip Goulder,[8,19] OPTIC consortium, ISARIC4C consortium, Elizabeth E. Fry,[2,*] Juthathip Mongkolsapaya,[4,5,*] Jingshan Ren,[2,*] David I. Stuart,[2,5,6,21,*] and Gavin R. Screaton[4,5,*]

[1]State Key Laboratory of Respiratory Disease, National Clinical Research Center for Respiratory Disease, Guangzhou Institute of Respiratory Health, the First Affiliated Hospital of Guangzhou Medical University, Guangzhou, Guangdong, China
[2]Division of Structural Biology, Nuffield Department of Medicine, University of Oxford, the Wellcome Centre for Human Genetics, Oxford, UK
[3]Guangzhou Laboratory, Bio-island, Guangzhou 510320, China
[4]Wellcome Centre for Human Genetics, Nuffield Department of Medicine, University of Oxford, Oxford, UK
[5]Chinese Academy of Medical Science (CAMS) Oxford Institute (COI), University of Oxford, Oxford, UK
[6]Diamond Light Source, Ltd., Harwell Science and Innovation Campus, Didcot, UK
[7]Oxford University Hospitals NHS Foundation Trust, Oxford, UK
[8]Peter Medawar Building for Pathogen Research, Oxford, UK
[9]Nuffield Department of Clinical Neurosciences, University of Oxford, Oxford, UK
[10]Translational Gastroenterology Unit, University of Oxford, Oxford, UK
[11]Oxford Vaccine Group, Department of Paediatrics, University of Oxford, Oxford, UK
[12]Department of Infection, Immunity and Cardiovascular Disease, University of Sheffield, Sheffield, UK
[13]Sheffield Teaching Hospitals NHS Foundation Trust, Sheffield, UK
[14]Viral Pseudotype Unit, Medway School of Pharmacy, University of Kent and Greenwich Chatham Maritime, Kent ME4 4TB, UK
[15]NIHR Oxford Biomedical Research Centre, Oxford, UK
[16]Centre for Tropical Medicine and Global Health, Nuffield Department of Medicine, University of Oxford, Oxford, UK
[17]Mahidol-Oxford Tropical Medicine Research Unit, Bangkok, Thailand
[18]Department of Medicine, University of Oxford, Oxford, UK
[19]Department of Paediatrics, University of Oxford, Oxford, UK
[20]These authors contributed equally
[21]Lead contact
*Correspondence: huojiandong@gird.cn (J.H.), liz@strubi.ox.ac.uk (E.E.F.), juthathip.mongkolsapaya@well.ox.ac.uk (J.M.), ren@strubi.ox.ac.uk (J.R.), dave@strubi.ox.ac.uk (D.I.S.), gavin.screaton@medsci.ox.ac.uk (G.R.S.)
https://doi.org/10.1016/j.celrep.2022.111903

SUMMARY

Variants of severe acute respiratory syndrome coronavirus 2 (SARS-CoV-2) have caused successive global waves of infection. These variants, with multiple mutations in the spike protein, are thought to facilitate escape from natural and vaccine-induced immunity and often increase in affinity for ACE2. The latest variant to cause concern is BA.2.75, identified in India where it is now the dominant strain, with evidence of wider dissemination. BA.2.75 is derived from BA.2 and contains four additional mutations in the receptor-binding domain (RBD). Here, we perform an antigenic and biophysical characterization of BA.2.75, revealing an interesting balance between humoral evasion and ACE2 receptor affinity. ACE2 affinity for BA.2.75 is increased 9-fold compared with BA.2; there is also evidence of escape of BA.2.75 from immune serum, particularly that induced by Delta infection, which may explain the rapid spread in India, where where there is a high background of Delta infection. ACE2 affinity appears to be prioritized over greater escape.

INTRODUCTION

Severe acute respiratory syndrome coronavirus 2 (SARS-CoV-2), the causative agent of coronavirus disease 2019 (COVID-19), has caused a devastating global pandemic, resulting in more than half a billion reported cases (probably greatly underestimating the number of infections) and over 6.4 million deaths as of August 2022 (https://covid19.who.int/). As a positive-strand RNA virus, although its replication machinery contains a proofreading exonuclease, SARS-CoV-2 has a high viral replication error rate.[1] This, combined with the massive scale of the pandemic and chronic infection in immunocompromised

individuals,[2] has generated mutational changes that endow viral fitness. The spike (S) gene, in particular, is the site of intense mutational change and selection,[3] and the encoded S protein, the major viral surface glycoprotein, is the principal antigenic target of all SARS-CoV-2 vaccines[4] and monoclonal antibody therapeutics[5] in current use.

S is presented as elongated trimeric spikes protruding from the virion surface. S is subdivided into an N-terminal S1 domain, responsible for host cell adhesion, and a C-terminal S2 domain anchored in the viral membrane, responsible for membrane fusion and cell entry after cleavage from S1, allowing the viral RNA to enter the host cell cytoplasm and initiate viral replication.[6] S1 consists of an N-terminal domain (NTD) and the receptor-binding domain (RBD), which mediates interaction with the ACE2 receptor on the host cell surface. Although a number of neutralizing monoclonal antibodies (nmAbs) have been found to target the NTD, especially the NTD supersite,[7] the majority of the nmAbs, particularly the most potent broadly reactive, target the RBD,[8,9] including all those in clinical use.[10]

The RBD is thus under intense selective pressure, and mutational changes may endow the virus a fitness advantage by enhancing viral transmissibility via an increased binding affinity for ACE2[11] or to evade the humoral response by impairing binding of the nmAbs to the RBD.[12] The rapid genetic evolution of SARS-CoV-2 raises an immediate need to monitor and characterize the transmissibility of new variants and their capacity for immune evasion.

A large number of variants have emerged, several of which have been designated variants of concern (VoCs) (https://www.cdc.gov/coronavirus/2019-ncov/variants/variant-classifications.html). Some VoCs have caused successive waves of infection worldwide: Alpha,[13] then Delta,[14] and recently Omicron,[15] while Beta[16] in Southern Africa and Gamma in South America[17] have caused regional outbreaks without wide global spread.

Omicron has caused the largest number of infections in the UK, with over 2.6 million confirmed cases (including BA.1 and BA.2) reported (https://www.gov.uk/government/publications/covid-19-variants-genomically-confirmed-case-numbers/variants-distribution-of-case-data-17-june-2022). Over 30 mutations are found in Omicron S, including 15 substitutions in the RBD, leading to increased transmissibility[18] and widespread large reductions in neutralizing antibody titers.[15]

Soon after the identification of Omicron BA.1, a number of sublineages emerged; BA.1.1, containing an additional R346K mutation in RBD, at one point accounted for about 40% of Omicron sequences globally, and about 35%–60% in the UK and the USA,[19] but was soon outcompeted by BA.2. BA.2 contains 8 unique substitutions in S, 6 within the RBD, and lacks 13 mutations found in BA.1[20] and has become the dominant strain across the world (https://www.who.int/publications/m/item/weekly-epidemiological-update-on-covid-19—6-july-2022). Recently, BA.2.12.1 has been identified in multiple countries (https://www.who.int/en/activities/tracking-SARS-CoV-2-variants/) and caused a large regional outbreak in North America (58% of sequences as of May 25, 2022).[21] In April 2022, BA.4 and BA.5 (which have identical S sequences) were reported from South Africa and now account for the majority (particularly BA.5) of sequenced cases in many countries (https://www.who.int/publications/m/item/weekly-epidemiological-update-on-covid-19—6-july-2022).

In early May 2022, a new Omicron BA.2 sublineage designated BA.2.75 was reported in India (https://www.who.int/en/activities/tracking-SARS-CoV-2-variants/) and has spread to multiple countries, including the UK, the USA, Australia, Germany, and Canada. Here, we report the antigenic characterization of BA.2.75 compared with other Omicron sublineages. In India, confirmed cases of BA.2.75 have outcompeted BA.5 and increased steeply from less than 20% of the total in early July to nearly 70% in mid-August (https://cov-spectrum.org/explore/India/AllSamples/from=2022-07-01&to=2022-08-21/variants?variantQuery=nextcladePangoLineage%3ABA.2.75*&). We find that neutralization of BA.2.75 is reduced compared with BA.2 using a number of vaccine and immune sera, but reductions are not as great as those found with BA.4/5. However, sera from Delta-infected cases showed no neutralization of BA.2.75, which may underlie the evolution and emergence of BA.2.75 in India, which suffered a major Delta wave in 2021. Finally, perhaps the most striking change found in BA.2.75 is the affinity of ACE2/RBD interaction. BA.2.75 affinity is increased 9-fold compared with BA.2. BA.2.75 has the highest affinity of all the SARS-CoV-2 variants measured to date and the only subnanomolar affinity we have determined. The N460K mutation probably increases affinity for ACE2 and also reduces the binding of some potent neutralizing antibodies. However, affinity to ACE2 appears to be prioritized over neutralization escape as evidenced by the acquisition of the RBD reversion mutation R493Q, which increases ACE2 affinity but makes the virus more sensitive to neutralization by vaccine sera. The very high affinity of BA.2.75 for ACE2 may increase the transmissibility of BA.2.75.

RESULTS

The Omicron lineage BA.2.75

BA.2.75 contains multiple mutational changes in the S protein compared with BA.2, including four substitutions in the NTD (W152R, F157L, I210V, and G257S) and four in the RBD (D339H, G446S, N460K, and R493Q) (Figure 1). The RBD mutations impinge on major epitopes for neutralizing antibodies and are likely to modulate ACE2 binding. D339H represents a further evolution of the G339D mutation found in all previous Omicron variants that has been found to impair the binding of certain "right-flank" antibodies belonging to the IGHV1-69 family (e.g., Beta-49 and -50) and falls in the binding footprint of certain class 3 antibodies such as S309/sotrovimab.[15] G446S was found in BA.1, BA.1.1, and BA.3, but not in BA.2 and other BA.2 subvariants, and is also able to impair binding of certain class 3 antibodies binding the right shoulder such as REGN10987/imdevimab.[15] The R493Q reversion was also found in BA.4/5 and may make the virus more sensitive to neutralization by a number of class 1 and 2 antibodies binding the neck/left shoulder. This reversion may also increase the affinity for ACE2 (see below).

N460K is a mutation not seen in previous VoCs or Omicron sublineages, but it was found after *in vitro* (yeast display) evolution in RBD-62, which has an ultra-high ACE2 affinity (K_D = 16–18 pM).[11,15] N460K was found repeatedly in these screens and is presumed to increase affinity for ACE2.[11]

A

BA.1 A67V,Δ69-70,T95I,G142D,Δ143-145, N211I,Δ212, ins214EPE
BA.1.1 A67V,Δ69-70,T95I,G142D,Δ143-145, N211I,Δ212, ins214EPE
BA.2 T19I,Δ24-26,A27S, G142D, V213G
BA.2.75 T19I,Δ24-26,A27S, G142D, W152R,F157L,I210V, V213G, G257S
BA.3 A67V,Δ69-70,T95I,G142D, Δ143-145, N211I,Δ212
BA.4/5 T19I,Δ24-26,A27S, Δ69-70, G142D, V213G

BA.1 G339D, S371L,S373P,S375F, K417N,N440K,G446S
BA.1.1 G339D,R346K,S371L,S373P,S375F, K417N,N440K,G446S
BA.2 G339D, S371F,S373P,S375F,T376A,D405N,R408S,K417N,N440K
BA.2.75 G339H, S371F,S373P,S375F,T376A,D405N,R408S,K417N,N440K,G446S
BA.3 G339D, S371F,S373P,S375F, D405N, K417N,N440K,G446S
BA.4/5 G339D, S371F,S373P,S375F,T376A,D405N,R408S,K417N,N440K

BA.1 S477N,T478K, E484A, Q493R,G496S,Q498R,N501Y,Y505H
BA.1.1 S477N,T478K,E484A, Q493R,G496S,Q498R,N501Y,Y505H
BA.2 S477N,T478K,E484A, Q493R, Q498R,N501Y,Y505H
BA.2.75 N460K,S477N,T478K,E484A, Q498R,N501Y,Y505H
BA.3 S477N,T478K,E484A, Q493R, Q498R,N501Y,Y505H
BA.4/5 L452R, S477N,T478K E484A,F486V, Q498R,N501Y,Y505H

BA.1 T547K,D614G,H655Y,N679K,P681H,N764K,D796Y,N856K,Q954H,N969K,L981F
BA.1.1 T547K,D614G,H655Y,N679K,P681H,N764K,D796Y,N856K,Q954H,N969K,L981F
BA.2 D614G,H655Y,N679K,P681H,N764K,D796Y, Q954H,N969K
BA.2.75 D614G,H655Y,N679K,P681H,N764K,D796Y, Q954H,N969K
BA.3 D614G,H655Y,N679K,P681H,N764K,D796Y, Q954H,N969K
BA.4/5 D614G,H655Y,N679K,P681H,N764K,D796Y, Q954H,N969K

B

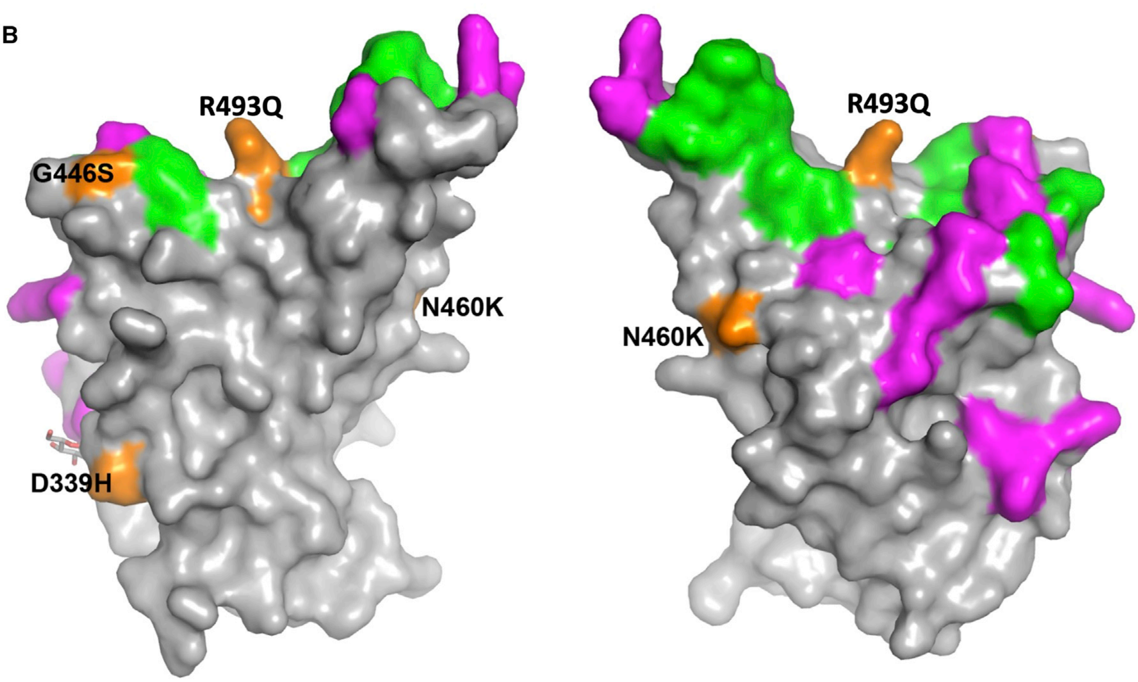

Figure 1. Sequence changes in BA.2.75 compared with other Omicron sublineages
(A) Sequence alignments of BA.2.75 together with Omicron sublineages Omicron BA.1, BA.1.1, BA.2, BA.3, and BA.4/5 boundaries of the NTD and RBD are marked.
(B) Surface representation of mutated residues in the BA.2.75 RBD compared with the BA.2 RBD. Positions of BA.2 RBD mutations (gray surface with the ACE2 footprint in dark green) are shown, and residues mutated in BA.2.75 are shown in orange and labeled.

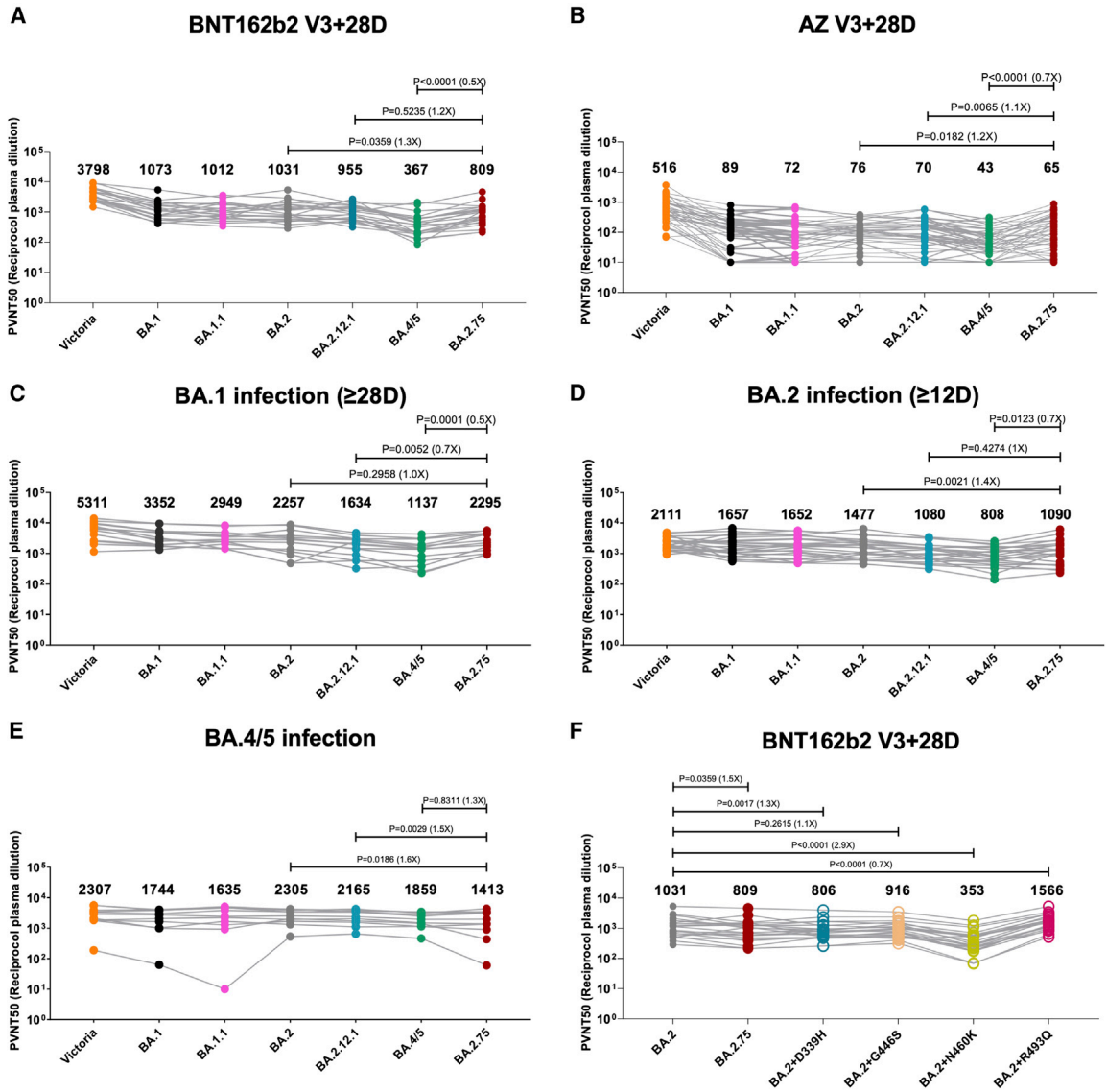

Figure 2. Pseudoviral neutralization assays of BA.2.75 by vaccine and BA.1, BA.2, and BA.4/5 immune serum

(A and B) IC50 values for the indicated viruses using serum obtained from vaccinees 28 days following their third dose of vaccine (A) Pfizer BNT162b2 (n = 22) or (B) AstraZeneca AZD AZD1222 (n = 41).

(C–E) Serum from volunteers suffering vaccine breakthrough BA.1 (n = 16), BA.2 (n = 23), or BA.4/5 (n = 11) infections.

(F) IC50 values for single RBD point mutations inserted into the BA.2 pseudovirus using Pfizer BNT162b2 serum (n = 22).

Geometric mean titers are shown above each column. The Wilcoxon matched-pairs signed rank test was used for the analysis and two-tailed p values were calculated.

See also Table S3.

Furthermore, our *in silico* analysis (below) suggests that N460K affects the binding of certain antibodies belonging to the IGHV3-53/66 families, which have been shown to be able to potently neutralize all VoCs.[20]

Neutralization of BA.2.75 by vaccine serum

We constructed a panel of pseudotyped lentiviruses[22] expressing the S gene from the Omicron sublineages BA.1, BA.1.1, BA.2, BA.2.12.1, BA.4/5, and BA.2.75 together with Victoria, an early pandemic Wuhan-related strain, used as control. We also included D339H, G446S, N460K, and R493Q as single mutations on the BA.2 background. Neutralization assays were performed using serum obtained 28 days following a third dose of the Oxford-AstraZeneca vaccine AZD1222 (n = 41)[23] or of Pfizer-BioNtech vaccine BNT162b2 (n = 22)[24] (Figure 2).

For BNT162b2, neutralization of BA.2.75 was reduced 1.3-fold compared with BA.2 ($p = 0.0359$) but increased 2.2-fold compared with BA.4/5 ($p < 0.0001$) (Figure 2A). For AZD1222, neutralization of BA.2.75 was reduced 1.2-fold compared with BA.2 ($p = 0.0182$) and 1.1-fold compared with BA.2.12.1

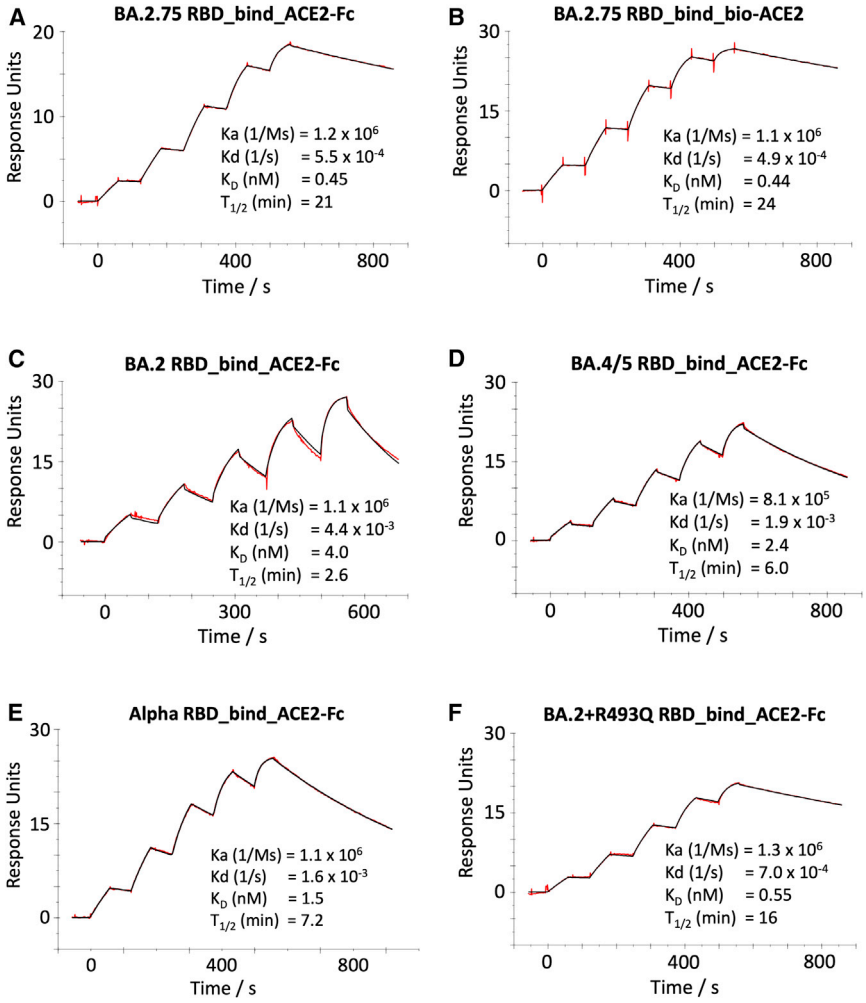

Figure 3. ACE2/RBD affinity

SPR sensorgrams showing ACE2 binding of BA.2.75 RBD using ACE2-Fc (A) or biotinylated ACE2 as ligand (B) compared with binding to the RBD of BA.2 (C), BA.4/5 (D), Alpha (E), and BA.2 + R493Q (F). The data for BA.2, BA.4/5, and Alpha have been reported previously in Tuekprakhon et al.,[12] Dejnirattisai et al.,[15] and Nutalai et al.,[20] respectively.

(p = 0.0065) but increased 1.5-fold compared with BA.4/5 (p < 0.0001) (Figure 2B). Overall, there are modest reductions in BA.2.75 neutralization titers of vaccine serum compared with BA.2 but not to the level seen with BA.4/5.

Neutralization of BA.2.75 by serum from vaccine breakthrough BA.1, BA.2, or BA.4/5 infections

Breakthrough BA.1 serum samples were taken from vaccinated volunteers ≥28 days from symptom onset (median, 38 days; n = 16). Pseudoviral neutralization assays were performed against the panel of pseudoviruses described above (Figure 2C). Neutralization titers for BA.2.75 were similar to BA.2 and 1.4- (p = 0.0052) and 2.0-fold (p = 0.0001) higher than BA.2.12.1 and BA.4/5, respectively.

Breakthrough BA.2 serum samples were taken from vaccinated volunteers ≥12 days from symptom onset (median, 29 days; n = 23). Pseudoviral neutralization assays were performed against the panel of pseudoviruses: Victoria, BA.1, BA.1.1, BA.2, BA.2.12.1, BA.4/5, and BA.2.75 (Figure 2D). Here, neutralization titers against BA.2.75 were modestly reduced compared with BA.2 (1.4-fold; p = 0.0021), similar to BA.2.12.1, but were still higher than BA.4/5 (0.7-fold; p = 0.0123). Taken together, BA.2.75 shows a modest degree of escape from humoral response induced by BA.2 breakthrough infection but not BA.1 infection.

Sequence-confirmed BA.4/5 infection serum samples were taken from 11 individuals (all but one vaccinated) >14 days (median, 38 days) (Figure 2E). Neutralization titers to BA.2.75 were 1.6-fold (p = 0.0186) reduced compared with BA.2 and reduced, but not significantly, in this relatively small sample compared with BA.4/5. These results are in line with the fact that the four new mutations found in BA.2.75 RBD are not shared with BA.2 or BA.4/5. Interestingly, although only a single case, the outlier in Figure 2E, which had essentially no neutralization of BA.1.1 (<50% neutralization at 1:20 serum dilution) and a low titer to BA.2.75 (7.7-fold reduced compared with BA.4/5), was from the unvaccinated case in this series; if this was representative of the response in the unvaccinated, it would suggest that unvaccinated individuals may be more susceptible to BA.2.75 infection following BA.4/5 infection.

Individual BA.2.75 mutations have differential effects on neutralization

To understand the effects of the individual mutations in the BA.2.75 RBD, we introduced them individually into the pseudovirus BA.2 background and assayed their neutralization using triple-vaccinated Pfizer BNT162b2 serum (Figure 2F). Neutralization titers for BA.2 were reduced for 3 of the 4 single-mutation variants of BA.2, with the greatest decrease for N460K (2.9-fold, p < 0.0001), followed by D339H (1.3-fold, p = 0.0006), and then by G446S (1.2-fold, p = 0.2312); however, neutralization titers were increased 1.5-fold by the R493Q reversion mutation (p < 0.0001). Q493 is present in all vaccines, thus explaining the increase in activity of vaccine serum to this reversion mutation.

ACE2/RBD binding affinities

We used surface plasmon resonance (SPR) to characterize the interaction between ACE2 and the BA.2.75 RBD. The off rate is slow, leading to a subnanomolar affinity (BA.2.75/ACE2

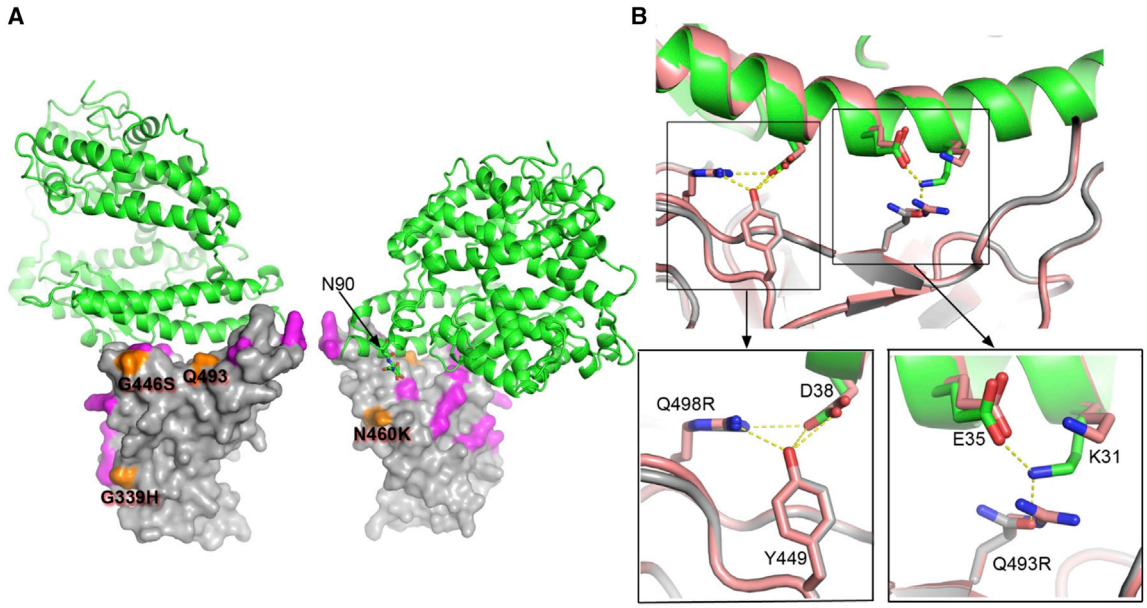

Figure 4. The structure of BA.2.75 RBD/ACE2 complex

(A) Front and back views of the overall structure of the BA.2.75 RBD/ACE2 complex. ACE2 is shown as green ribbons and the RBD as surface with mutations common to BA.2 highlighted in magenta and those that are different in orange.

(B) BA.2.75 RBD (gray) and ACE2 (green) interface compared with that of BA.2 and ACE2 (both in salmon). Close ups show interactions of Q498R and Q493 (R493 in BA.2) with ACE2.

See also Table S5.

K_D = 0.45 nM) (Figures 3A and 3B). This represents a considerable increase in affinity compared with BA.2 (9-fold) (Figure 3C) and is even tighter than BA.4/5 (5-fold) (Figure 3D), which was previously shown to bind ACE2 with higher affinity than BA.2.[12] Indeed, BA.2.75 is the strongest ACE2 binder among all SARS-CoV-2 VoCs, including Alpha (Alpha/ACE2 K_D = 1.5 nM; (Figure 3E), and is the only subnanomolar affinity we have measured. We were unable to express the BA.2 + N460K RBD, which is expected to contribute to the increased affinity, but we measured the binding affinity of the BA.2 + R493Q RBD to ACE2 (K_D = 0.55 nM) (Figure 3F), confirming that the reversion mutation contributes to the high affinity of the BA.2.75 RBD.

ACE2/BA.2.75 RBD structure

To elucidate the molecular mechanism for high affinity, we determined the structure of the BA.2.75 RBD with ACE2 by crystallography (see STAR Methods). As expected, the binding mode was essentially indistinguishable from that observed before (Figure 4A), although there were significant rearrangements outside of the ACE2 footprint, with the flexible RBD 371–375 loop rearranging and part of the C-terminal 6×His tag becoming ordered. Figure 4B shows a close up of the binding interface compared with the ACE2/BA.2 RBD complex. We note that in other complexes (with either R or Q at RBD 493), K31 of ACE2 tends to be disordered, whereas it is well ordered in the BA.2.75 complex, allowing K31 to form a potential hydrogen bond with the glutamine 493 side chain of the RBD, possibly increasing the affinity of ACE2. Although N460K is outside of the footprint of ACE2 on the RBD (Figure 4A), evidence from *in vitro* evolution suggests that it probably increases the affinity for ACE2.[11] This is probably due to the improved electrostatic match,[11] although we also note that the density map for RBD-62 with ACE2[11] (EMDB: 12187) suggests that the glycan attached to N90 of ACE2 makes a direct interaction with the RBD close to residue 460.

Escape from mAbs by BA.2.75

To dissect how BA.2.75 might affect neutralizing antibody activity, we used pseudoviral assays to test a recently reported panel of potent human mAbs generated from cases of Omicron breakthrough infection (BA.1 IC50 titers <0.1 μg/mL)[20] (Figure 5A; Table S1A). Among the 27 RBD-specific mAbs, those belonging to the IGHV3-53/66 families are the most severely affected. Three (Omi-16, Omi-29, and Omi-36) showed a complete knockout of BA.2.75 neutralization; an additional four (Omi-18, Omi-20, Omi-27, and Omi-28) showed >5-fold reduction compared with BA.2, which is in line with the observation that N460 interacts very closely with the highly conserved GGS/T CDR-H2 motif found in many IGHV-3/66 antibodies.

Structures for two representative mAbs, Omi3 and Omi-18, in Figures 6A and 6B[14,17,20] indicate that the larger lysine side chain of the N460K mutation will interfere with binding. Like BA.2 and BA.4/5, BA.2.75 is not neutralized by the anti-NTD mAb Omi-41, which only interacts with the NTDs of BA.1, BA.1.1, and BA.3.

The Omi mAbs were also tested against the pseudoviruses encoding single point mutations in the BA.2 RBD described above (Figure S1; Table S2). As expected, the IGHV3-53/66 mAbs that lost neutralization to BA.2.75 were also impacted by the N460K

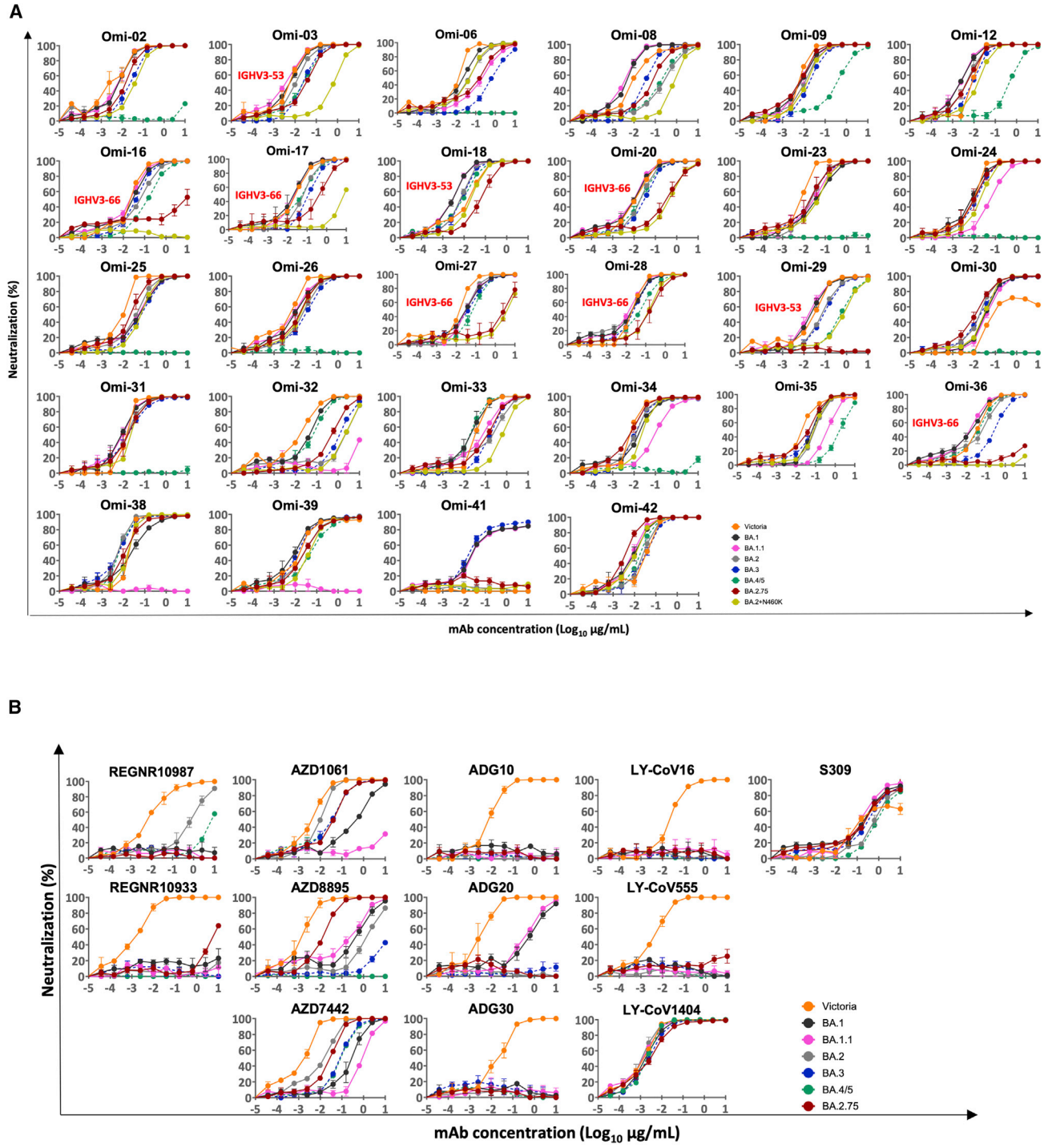

Figure 5. Pseudoviral neutralization assays against monoclonal antibodies

(A) Neutralization curves for a panel of 28 mAbs made from samples taken from vaccinees infected with BA.1. Titration curves for BA.2.75 are compared with Victoria, BA.1, BA.1.1, BA.2, and BA.4/5. IC50 titers are shown in Table S1A.

(B) Pseudoviral neutralization assays with mAbs developed for human use. IC50 titers are shown in Table S1B. Data for Victoria, BA.1, BA.1.1, BA.2, and BA.4/5 are used for comparison and are taken from Tuekprakhon et al.[12]

See also Figure S1. All assays have been done at least twice.

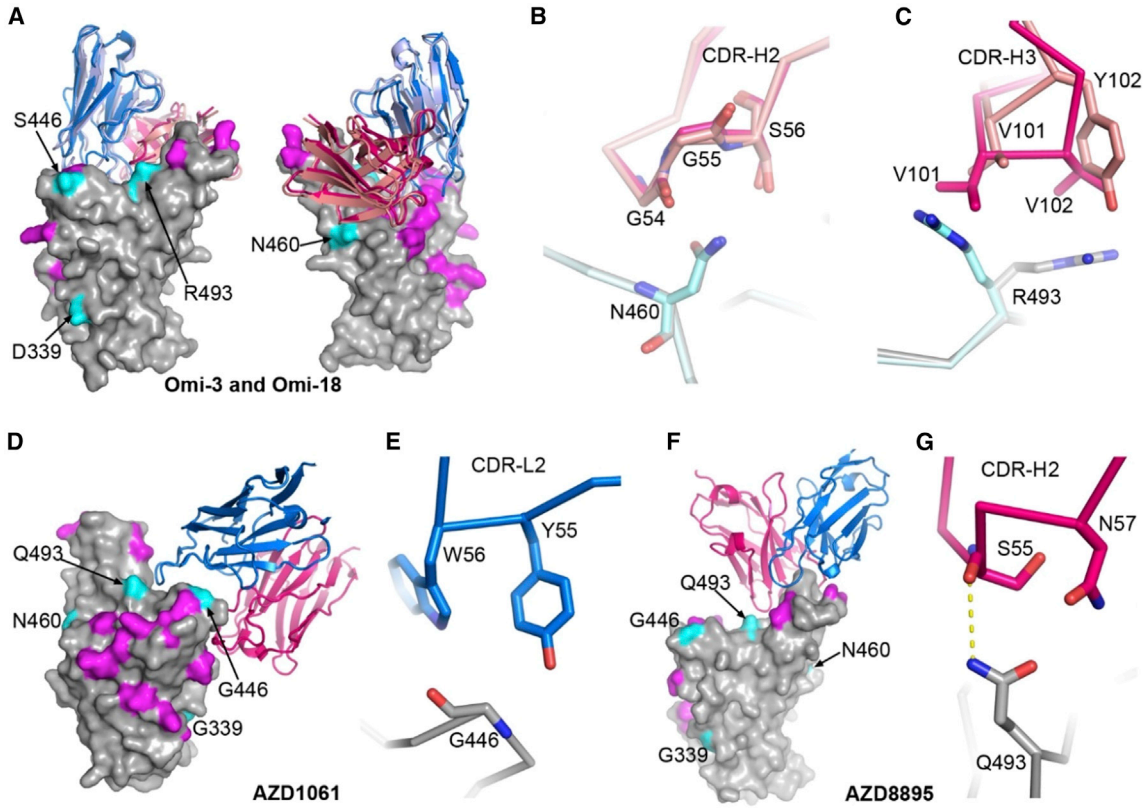

Figure 6. Interactions between mAbs and BA.2.75 mutation sites

(A) Front and back views of the binding modes of Omi-3 (PDB: 7ZF3) and Omi-18 (PDB: 7ZFC) complexed with Omicron BA.1 RBD by overlapping the RBD. The RBD is shown as a gray surface representation with mutations common to both BA.2 and BA.2.75 colored in magenta, and the four mutations that differ between the two are in cyan. Vhs and Vls are shown as ribbons and colored in red and blue for Omi-3 and light blue and salmon for Omi-18, respectively.

(B) Interactions between N460 of the RBD and CDR-H2 of the Fabs.

(C) Contacts between R493 of the RBD and CDR-H3 of the Fabs.

In (B and C), the RBD associated with Omi-3 is in gray and Omi-18 in cyan, and the colors of the Fabs are as in (A).

(D and E) AZD1061 bound with the ancestral SARS-CoV-2 RBD (PDB: 7L7E) (D) and contacts between G446 of the RBD and CDR-L2 of the Fab (E).

(F and G) AZD8895 bound with the ancestral SARS-CoV-2 spike RBD (PDB: 7L7E) (F) and contacts between Q493 of the RBD and CDR-H2 of the Fab (G).

In (D–F), the RBD is drawn and colored as in (A), and heavy chain is in red and light chain in blue.

mutation, confirming the prediction that this residue was critical for the binding of a number of this public gene family. Interestingly, The BA.2 + N460K mutation in isolation shows a larger impact than the full BA.2.75 complement of S mutations on the activity of several mAbs: the neutralization titer of Omi-3 (IGHV3-53) was reduced 50-fold for BA.2 + N460K but only 2-fold for BA.2.75; Omi-17 (IGHV3-66) was completely knocked out on BA.2 + N460K but only reduced 4-fold for BA.2.75; and Omi-33 (IGHV3-33) was reduced 7-fold for BA.2 + N460K, but there was no change observed for BA.2.75. Thus, other mutations in BA.2.75 might have mitigated the effect of the N460K mutation, particularly the R493Q mutation, which has a different impact on various IGHV gene families and even differs within the IGHV3-53/66 family (Figure 6C). However, we cannot fully explain the marked differences of effect observed for the impact of the 460 mutations between Omi-3 and Omi-18 (Figure S1; Table S2), since the contacting GGS/T CDR-H2 motif is structurally almost identical between these two mAbs (Figure 6B). Interestingly, BA.2.75 is more sensitive to Omi-32 (IGHV3-33) than is BA.2, with an 8-fold increase in neutralization titer (Figure 5A; Table S1).

To confirm that the changes in neutralizing activities observed are associated with alterations in RBD interaction, we performed binding analyses of selected antibodies to BA.2.75 and BA.2 RBDs by SPR (Figure S2). Binding of Omi-29 (IGHV3-53) and Omi-36 (IGHV3-66) to BA.2.75 was severely impaired, and Omi-18 and Omi-20 showed 8-fold reductions compared with BA.2. On the other hand, a 2-fold increase in binding affinity of Omi-32 was seen for BA.2.75 compared with BA.2, in line with the enhanced neutralization titer observed (above).

Effect of commercial monoclonals against BA.2.75

We evaluated the sensitivity of a panel of mAbs that have been developed as therapeutics against BA.2.75 (Figure 5B; Table S1B). The neutralization profiles are, in general, similar between BA.2.75 and BA.2; however, further to the 6/12 mAbs (REGN10933, ADG10, ADG20, ADG30, LY-CoV555, LY-CoV16), which have already suffered complete loss of

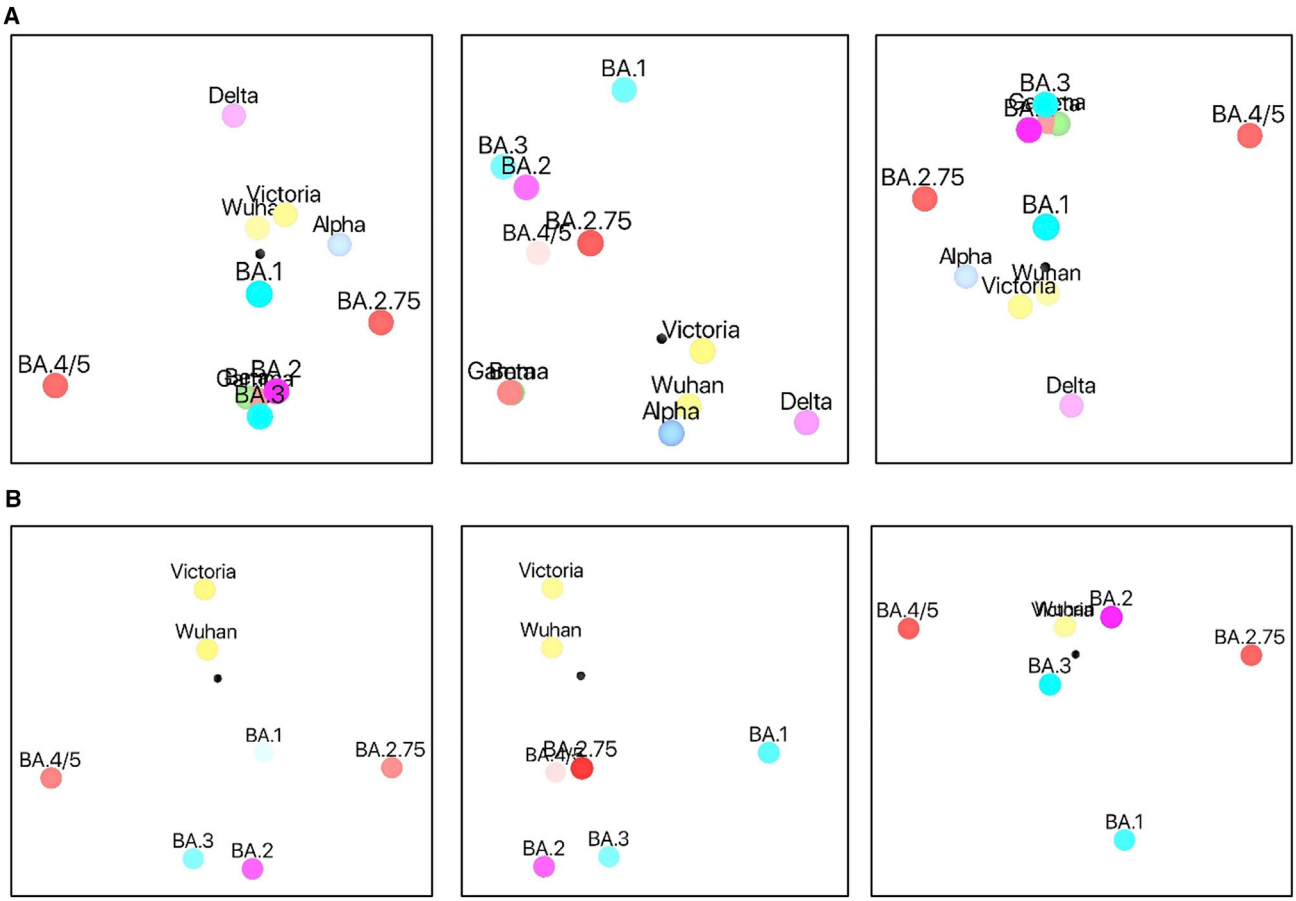

Figure 7. Antigenic mapping

(A) Orthogonal views of the antigenic map showing BA.2.75 in the context of the positions of early pandemic viruses, previous VoCs, and Omicron sublineages calculated from pseudovirus neutralization data. Distance between two positions is proportional to the reduction in neutralization titer when one of the corresponding strains is challenged with serum derived by infection by the other. No scale is provided since the figures are projections of a 3D distribution; however, the variation can be calibrated by comparison with (1) BA.1 to BA.2, which is 2.93× reduced, and (2) BA.2 to BA.4/5, which is 3.03× reduced.

(B) As (A) but including only Omicron sublineages and early pandemic viruses to allow more accurate projection of this subset into three dimensions. Note that responses of these viruses against all sera were included in the calculations.

See also Table S1.

neutralizing activity for BA.2, the residual activity of REG10987[25] against BA.2 was further knocked out for BA.2.75 due to the G446S mutation.[15] For AZD1061, activity against BA.2.75 was similar to that against BA.2 (<3-fold reduction), while the AZD8895 titer was restored to 8 ng/mL for BA.2.75 from 1,333 ng/mL for BA.2, a 167-fold increase in activity. As a result, AZD7442 (a combination of AZD8895 and AZD1061)[26] showed similar activity against BA.2.75 and BA.2 (2-fold reduction). The results can be explained by the structure of the ternary complex of the ancestral SARS-CoV-2 RBD/AZD1061/AZD8895.[26] G446 has contacts with CDR-L2 Y55 and W56 of AZD1061, thus the G446S mutation will induce steric clashes (Figures 6D and 6E), and while the CDR-H2 of AZD8895 sits above and makes a hydrogen bond to Q493 of the RBD, an arginine at 493 will severely clash with the CDR-H2 (Figures 6F and 6G). The activity of S309[27] is increased 3-fold for BA.2.75 compared with BA.2, suggesting that the D339H mutation in BA.2.75 reduces the impact of the preceding G339D mutation in BA.2 on the activity of S309. LY-CoV1404 (bebtelovimab)[28] is the only mAb where neutralization is fully retained on all Omicron sublineages.

Antigenic mapping

We tested the neutralization of BA.2.75 using serum from previously infected individuals. This included serum obtained early in the pandemic (before the emergence of Alpha) together with sera obtained following Alpha, Beta, Gamma, Delta, BA.1, and BA.2 infections (Figure S3). As expected, BA.2.75 neutralization titers were lower than the homologous infecting strain (e.g., Alpha serum on the Alpha strain). Most striking, however, was the complete loss of BA.2.75 neutralization using Delta serum (zero samples achieved 50% neutralization at 1/20 dilution). However, titers to BA.2.75 were much higher in cases who had been vaccinated before or after Delta infection.

We used these data to place BA.2.75 onto a 3D antigenic map using the method we have previously reported[12] (Figures 7A and 7B; Videos S1 and S2). Initially, all VoCs

were included (Figure 7A; Video S1); BA.2.75 forms part of the constellation of Omicron viruses, which segregate into one hemisphere of the 3D plot. BA.2.75 is well separated from other Omicron sublineages and especially from BA.4/5. It is notable that BA.2.75 and Delta are diametrically opposed in the diagram, emphasizing the antigenic distance between these two viruses. Since the data are higher dimensional, this 3D projection is likely to distort the true distances, and so we recalculated the map only for the Omicron lineage and early pandemic viruses (but retain the fully serology information for these). The results are shown in Figure 7B and Video S2 and recapitulate the major features of the plot containing the other VoCs but allow the Omicron sublineages to distribute more broadly in 3D space. It is remarkable that if we consider the two early pandemic viruses as a single point, and likewise merge BA.2 and BA.3 pairs, then the points are distributed as a trigonal bipyramid, maximizing their separation, consistent with antigenic escape being a significant factor in their evolution.

DISCUSSION

Following the designation of Omicron as a VoC in November 2021, a succession of sublineages emerged, including BA.1.1, BA.2, BA.2.12.1, and BA.4/5, which have outcompeted preceding strains to become regionally or globally dominant. Since June 2022, BA.4/5, which has both higher receptor binding affinity and a markedly enhanced escape from antibody responses,[12] quickly spread from South Africa across the world and has now become the new globally dominant strain, with BA.5 in the ascendency in many regions.

Very recently, a new Omicron sublineage designated as BA.2.75 has emerged in India and spread to many countries. The true prevalence of BA.2.75 is difficult to determine as sequencing in many countries is patchy and has, in recent months, been greatly scaled back. However, in India, BA.2.75 has rapidly outcompeted BA.4/5 to recently become the dominant variant. Here, we show reductions in neutralization titers to BA.2.75 of triple-dosed BNT162b2 and AZD1222 vaccine serum compared with BA.2, but the reductions in BA.2.75 neutralization are less pronounced than BA.4/5. For serum derived from BA.1 breakthrough infection in vaccinated individuals, the BA.2.75 titers are similar to BA.2. However, we find that BA.2.75 neutralization titers are modestly lower (1.3-fold) than BA.2 for BA.2 breakthrough serum and are 1.6-fold reduced compared with BA.2 for BA.4/5-infected serum, and if the results on BA.2.75 neutralization by BA.4/5 from a single unvaccinated case were replicated on a larger scale, it would suggest that such individuals would be more at risk of BA.2.75 infection.

Overall, the constellation of mutations in BA.2.75 compared with BA.2 have opposing effects on neutralization, the reversion mutation R493Q makes the virus easier to neutralize using vaccine serum (the vaccine contains Q493), while N460K reduces neutralization titers to a greater extent when expressed in isolation compared with the combination of mutations seen in BA.2.75. N460K is a substitution that has not appeared in preceding variants of SARS-CoV-2. When we introduced N460K into the BA.2 backbone, BA.2 + N460K titers were reduced 2.9-fold compared with BA.2, which is greater than the reduction seen with BA.2.75 and on a par with the reduction seen for BA.4/5, using BNT162b2 triple-vaccinated serum.

Dissecting these effects using a panel of potent mAbs derived from vaccinated individuals who suffered BA.1 vaccine breakthrough infection, we show that those belonging to the IGHV3-53/66 family are reduced or knocked out against BA.2.75. IGHV3-53/66 are the most frequently isolated mAbs in SARS-CoV-2 and bind an epitope on the "neck."[17] IGHV3-53/66 thus forms a major public antibody response, and it is no surprise that the virus has evolved to escape this response. Mutations found in previous VoCs lead to loss of function of many IGHV53/66 mAbs, but this antibody class has proved to be very adaptable to accommodate change,[20] and it would seem likely that somatic mutation will allow the response to adapt to the N460K mutation following BA.2.75 infection.

Interestingly, BA.2.75 has also acquired the R493Q reversion (Q493R was acquired in BA.1 and present in all other Omicron sublineages except BA.4/5). Here, we show that the BA.2.75 RBD is able to bind ACE2 with 9-fold higher affinity than BA.2 and more tightly than BA.4/5.[12,15] BA.2.75 has the highest ACE2 affinity among all SARS-CoV-2 variants we have measured to date, and we show that this is partly attributable to the R493Q mutation. Although we have been unable to express the BA.2 + N460K RBD, previous studies show that N460K can enhance RBD binding for ACE2, an effect similar in magnitude to that seen with the N501Y mutation described initially in Alpha;[11] thus N460K probably both enhances antibody escape and increases receptor binding affinity.

There is likely a fine interplay between antibody escape and ACE2 receptor affinity; Alpha (N501Y) evolved early during the pandemic, when the background population SARS-CoV-2 exposure was relatively low. Although neutralization titers against Alpha were modestly reduced compared with ancestral strains,[29] it is likely that the major driver for the evolution of Alpha N501Y was an increase in ACE2 affinity, giving the virus a transmission advantage.[30] Currently, population exposure to SARS-CoV-2 by either natural infection or vaccination is high, leading to the dual pressure of increased ACE2 affinity and antibody evasion. For the R493Q reversion, the balance between a reduction in antibody escape but increased ACE2 affinity may have tipped to allow BA.2.75 to more effectively transmit in certain populations. Other factors such as S stability, replication time, and reduced TMPRSS2 dependence also influence the success of SARS-CoV-2 variants.[30–33]

BA.2.75 has become the dominant SARS-CoV-2 strain in India, and it will soon become clear whether BA.2.75 is able to outcompete BA.4/5 to become the globally dominant strain or whether it will remain regionally localized, as was the case for Beta and Gamma. If the latter, it may reflect the different background immunity of the population. India, where BA.2.75 seems to have originated, has a very high background of Delta infection. Using neutralization assays, we show that Delta infection in isolation provides no protection (no neutralization) against BA.2.75. In other countries where vaccination programs are more advanced, together with the high level of Omicron immunity, there may be sufficient protection to check BA.2.75.

Very recently, a number of new variants have been emerging based upon BA.5 or BA.2.75, including BA.2.3.20, BA.2.75.2,

BA.2.10.4, and BJ.1, among others; these variants have picked up a host of additional mutations in the RBD, with evidence of co-evolution of a number of residues, and appear to be selected to increase escape from Omicron neutralizing serum (https://www.biorxiv.org/content/10.1101/2022.09.15.507787v3).

In summary, we show the mutations in BA.2.75 lead to a reduction in neutralization titers of vaccine serum compared with BA.2. Individual BA.2.75 mutations can cause greater reduction in neutralization titers compared with the full BA.2.75 S sequence, but these are balanced by the R493Q reversion mutation, which may have been selected to increase affinity to ACE2 and increase the transmissibility of BA.2.75. It seems inevitable that further evolution of the Omicron lineage will occur, and there are likely many possible trade-offs between antibody escape and ACE2 affinity that can and will be made, leading to successive waves of infection.

Limitations of the study

Limitations of this study are that the *in vitro* neutralization assays we used do not probe the full function of the antibody response, as they do not measure the effects of complement- or antibody-dependent cell-mediated cytotoxicity, which both operate *in vivo*. In addition, as live BA.2.75 virus was not available in our laboratory, we relied on lentiviral pseudoneutralization assays for characterization. Furthermore, they do not take account of T cell responses, which have been shown to be more resilient to the mutations expressed by VoCs.

CONSORTIA

The members of OPTIC are Christopher Conlon, Alexandra Deeks, John Frater, Lisa Frending, Siobhan Gardiner, Anni Jämsén, Katie Jeffery, Tom Malone, Eloise Phillips, Lucy Rothwell, and Lizzie Stafford.

STAR★METHODS

Detailed methods are provided in the online version of this paper and include the following:

- KEY RESOURCES TABLE
- RESOURCE AVAILABILITY
  - Lead contact
  - Materials availability
  - Data and code availability
- EXPERIMENTAL MODEL AND SUBJECT DETAILS
  - Bacterial strains and cell culture
  - Plasma from early pandemic and Alpha cases
  - Sera from BA.4/5 infected cases, study subjects
  - Sera from Beta, Gamma and Delta infected cases
  - *Sera from BA.1 infected cases,* study subjects
  - *Sera from BA.2 infected cases,* study subjects
  - Sera from Pfizer vaccinees
  - AstraZeneca-Oxford vaccine study procedures and sample processing
- METHOD DETAILS
  - Pseudovirus plasmid construction and lentiviral particles production
  - Pseudoviral neutralization test
  - Cloning of RBDs
  - Production of RBDs
  - Surface plasmon resonance
  - IgG mAbs and Fabs production
  - Crystallization, X-Ray data collection and structure determination
  - Antigenic mapping
- QUANTIFICATION AND STATISTICAL ANALYSIS

SUPPLEMENTAL INFORMATION

Supplemental information can be found online at https://doi.org/10.1016/j.celrep.2022.111903.

ACKNOWLEDGMENTS

This work was supported by the Chinese Academy of Medical Sciences (CAMS) Innovation Fund for Medical Science (CIFMS), China (grant number: 2018-I2M-2-002), to D.I.S. and G.R.S. We are also grateful for support from Schmidt Futures, the Red Avenue Foundation, and the Oak Foundation. G.R.S. was supported by Wellcome. H.M.E.D., and J.R. are supported by Wellcome (101122/Z/13/Z) and D.I.S. and E.E.F. by the UKRI MRC (MR/N00065X/1). D.I.S. and G.R.S. are Jenner investigators. This is a contribution from the UK Instruct-ERIC Center. A.J.M. is an NIHR-supported academic clinical lecturer. The convalescent sampling was supported by the Medical Research Council (grant MC_PC_19059 awarded to the ISARIC4C Consortium with a full contributor list available at https://isaric4c.net/about/authors/), the National Institutes of Health, Oxford Biomedical Research Centre, and an Oxfordshire Health Services Research Committee grant to A.J.M. The Wellcome Center for Human Genetics is supported by the Wellcome Trust (grant 090532/Z/09/Z). The computational aspects of this research were supported by the Wellcome Trust Core Award grant number 203141/Z/16/Z and the NIHR Oxford BRC. The Oxford Vaccine work was supported by UK Research and Innovation, Coalition for Epidemic Preparedness Innovations, National Institute for Health Research (NIHR), NIHR Oxford Biomedical Research Centre, Thames Valley and South Midland's NIHR Clinical Research Network. We thank the Oxford Protective T-cell Immunology for COVID-19 (OPTIC) clinical team for participant sample collection and the Oxford Immunology Network COVID-19 Response T cell Consortium for laboratory support. We acknowledge the rapid sharing of Victoria, B.1.1.7, and B.1.351, which were isolated by scientists within the National Infection Service at PHE Porton Down, and the B.1.617.2 virus was kindly provided Wendy Barclay and T.I.d.S. We thank The Secretariat of National Surveillance, Ministry of Health Brazil, for assistance in obtaining P.1 samples. This work was supported by the UK Department of Health and Social Care as part of the PITCH (Protective Immunity from T Cells to Covid-19 in Health Workers) Consortium, the UK Coronavirus Immunology Consortium (UK-CIC), and the Huo Family Foundation. We acknowledge Diamond Light Source for time on Beamline I03 under Proposal lb27009 for COVID-19 Rapid Access. We thank the staff of the MRC Human Immunology Unit for access to their Biacore Facility. E.B. and P.K. are NIHR Senior Investigators, and P.K. is funded by WT222426/Z/21/Z and NIH (U19 I082360). S.J.D. is funded by an NIHR Global Research Professorship (NIHR300791). D.S. is an NIHR Academic Clinical Fellow. The Sheffield Teaching Hospitals Observational Study of Patients with Pulmonary Hypertension, Cardiovascular and Other Respiratory Diseases (STH-ObS) was supported by the British Heart Foundation (PG/11/116/29288). The STH-ObS Chief Investigator Allan Lawrie is supported by a British Heart Foundation Senior Basic Science Research fellowship (FS/18/52/33808). We gratefully acknowledge financial support from the UK Department of Health via the Sheffield NIHR Clinical Research Facility award to the Sheffield Teaching Hospitals Foundation NHS Trust. The views expressed in this article are those of the authors and not necessarily those of the National Health Service (NHS), the Department of Health and Social Care (DHSC), the National Institutes for Health Research (NIHR), the Medical Research Council (MRC), or Public Health, England.

AUTHOR CONTRIBUTIONS

J.H. performed interaction affinity analyses. D.Z. performed antibody competition analyses. D.Z., J.H., J.R., N.G.P., M.A.W., and D.R.H. prepared the crystals and enabled and performed X-ray data collection. J.R., E.E.F., H.M.E.D., and D.I.S. analyzed the structural results. G.R.S., J.H., J.M., P.S., D.Z., R.N., A.T., A.D.-G., M.S., R.D., and C.L. prepared the RBDs, ACE2, and antibodies, and C.L. and P.S. performed neutralization assays. N.T. provided materials. H.M.G. wrote mabscape and performed mapping and cluster analysis, including sequence and antigenic space analyses. A.J.M., D.S., T.G.R., A.A., S.B., S.A., S.A.J., P.K., E.B. S.J.D., A.J.P., T.L., and P.G. assisted with patient samples and vaccine trials. E.B., S.J.D., and P.K. conceived the study of vaccinated healthcare workers and oversaw the OPTIC Healthcare Worker study and sample collection/processing. T.I.d.S, M.P., T.A.H.N., and H.H. assisted with healthcare worker recruitment and sample collection in the Sheffield STH-ObS study. G.R.S. and D.I.S. conceived the study. G.R.S., D.I.S., and J.H. wrote the initial manuscript draft with other authors providing editorial comments. All authors read and approved the manuscript.

DECLARATION OF INTERESTS

G.R.S. sits on the GSK Vaccines Scientific Advisory Board, consults for Astra Zeneca, and is a founding member of RQ Biotechnology. Oxford University holds intellectual property related to the Oxford-Astra Zeneca vaccine and SARS-CoV-2 mAbs discovered in G.R.S.'s laboratory. A.J.P. is Chair of UK Dept. Health and Social Care's (DHSC) Joint Committee on Vaccination & Immunisation (JCVI) but does not participate in the JCVI COVID-19 committee and is a member of the WHO's SAGE. The views expressed in this article do not necessarily represent the views of DHSC, JCVI, or WHO. The University of Oxford has entered into a partnership with AstraZeneca on coronavirus vaccine development. T.L. is named as an inventor on a patent application covering this SARS-CoV-2 vaccine and was a consultant to Vaccitech for an unrelated project whilst the study was conducted. S.J.D. is a scientific advisor to the Scottish Parliament on COVID-19.

Received: September 14, 2022
Revised: November 5, 2022
Accepted: December 8, 2022

REFERENCES

1. Robson, F., Khan, K.S., Le, T.K., Paris, C., Demirbag, S., Barfuss, P., Rocchi, P., and Ng, W.L. (2020). Coronavirus RNA proofreading: molecular basis and therapeutic targeting. Mol. Cell *79*, 710–727.
2. Greninger, A.L., Dien Bard, J., Colgrove, R.C., Graf, E.H., Hanson, K.E., Hayden, M.K., Humphries, R.M., Lowe, C.F., Miller, M.B., Pillai, D.R., et al. (2022). Clinical and infection prevention applications of severe acute respiratory syndrome coronavirus 2 genotyping: an infectious diseases society of America/American society for microbiology consensus review document. J. Clin. Microbiol. *60*, e0165921.
3. Obermeyer, F., Jankowiak, M., Barkas, N., Schaffner, S.F., Pyle, J.D., Yurkovetskiy, L., Bosso, M., Park, D.J., Babadi, M., MacInnis, B.L., et al. (2022). Analysis of 6.4 million SARS-CoV-2 genomes identifies mutations associated with fitness. Science *376*, 1327–1332.
4. Sadeghalvad, M., Mansourabadi, A.H., Noori, M., Nejadghaderi, S.A., Masoomikarimi, M., Alimohammadi, M., and Rezaei, N. (2022). Recent developments in SARS-CoV-2 vaccines: a systematic review of the current studies. Rev. Med. Virol., e2359.
5. Focosi, D., McConnell, S., Casadevall, A., Cappello, E., Valdiserra, G., and Tuccori, M. (2022). Monoclonal antibody therapies against SARS-CoV-2. Lancet Infect. Dis. *22*, e311–e326.
6. Walls, A.C., Tortorici, M.A., Snijder, J., Xiong, X., Bosch, B.J., Rey, F.A., and Veesler, D. (2017). Tectonic conformational changes of a coronavirus spike glycoprotein promote membrane fusion. Proc. Natl. Acad. Sci. USA *114*, 11157–11162.
7. Lok, S.M. (2021). An NTD supersite of attack. Cell Host Microbe *29*, 744–746.
8. Niu, L., Wittrock, K.N., Clabaugh, G.C., Srivastava, V., and Cho, M.W. (2021). A structural landscape of neutralizing antibodies against SARS-CoV-2 receptor binding domain. Front. Immunol. *12*, 647934.
9. Piccoli, L., Park, Y.J., Tortorici, M.A., Czudnochowski, N., Walls, A.C., Beltramello, M., Silacci-Fregni, C., Pinto, D., Rosen, L.E., Bowen, J.E., et al. (2020). Mapping neutralizing and immunodominant sites on the SARS-CoV-2 spike receptor-binding domain by structure-guided high-resolution serology. Cell *183*, 1024–1042.e21.
10. Corti, D., Purcell, L.A., Snell, G., and Veesler, D. (2021). Tackling COVID-19 with neutralizing monoclonal antibodies. Cell *184*, 4593–4595.
11. Zahradník, J., Marciano, S., Shemesh, M., Zoler, E., Harari, D., Chiaravalli, J., Meyer, B., Rudich, Y., Li, C., Marton, I., et al. (2021). SARS-CoV-2 variant prediction and antiviral drug design are enabled by RBD in vitro evolution. Nat. Microbiol. *6*, 1188–1198.
12. Tuekprakhon, A., Nutalai, R., Dijokaite-Guraliuc, A., Zhou, D., Ginn, H.M., Selvaraj, M., Liu, C., Mentzer, A.J., Supasa, P., Duyvesteyn, H.M.E., et al. (2022). Antibody escape of SARS-CoV-2 Omicron BA.4 and BA.5 from vaccine and BA.1 serum. Cell *185*, 2422–2433.e13.
13. Supasa, P., Zhou, D., Dejnirattisai, W., Liu, C., Mentzer, A.J., Ginn, H.M., Zhao, Y., Duyvesteyn, H.M.E., Nutalai, R., Tuekprakhon, A., et al. (2021). Reduced neutralization of SARS-CoV-2 B.1.1.7 variant by convalescent and vaccine sera. Cell *184*, 2201–2211.e7.
14. Liu, C., Ginn, H.M., Dejnirattisai, W., Supasa, P., Wang, B., Tuekprakhon, A., Nutalai, R., Zhou, D., Mentzer, A.J., Zhao, Y., et al. (2021). Reduced neutralization of SARS-CoV-2 B.1.617 by vaccine and convalescent serum. Cell *184*, 4220–4236.e13.
15. Dejnirattisai, W., Huo, J., Zhou, D., Zahradník, J., Supasa, P., Liu, C., Duyvesteyn, H.M.E., Ginn, H.M., Mentzer, A.J., Tuekprakhon, A., et al. (2022). SARS-CoV-2 Omicron-B.1.1.529 leads to widespread escape from neutralizing antibody responses. Cell *185*, 467–484.e15.
16. Zhou, D., Dejnirattisai, W., Supasa, P., Liu, C., Mentzer, A.J., Ginn, H.M., Zhao, Y., Duyvesteyn, H.M.E., Tuekprakhon, A., Nutalai, R., et al. (2021). Evidence of escape of SARS-CoV-2 variant B.1.351 from natural and vaccine-induced sera. Cell *184*, 2348–2361.e6.
17. Dejnirattisai, W., Zhou, D., Supasa, P., Liu, C., Mentzer, A.J., Ginn, H.M., Zhao, Y., Duyvesteyn, H.M.E., Tuekprakhon, A., Nutalai, R., et al. (2021). Antibody evasion by the P.1 strain of SARS-CoV-2. Cell *184*, 2939–2954.e9.
18. Suzuki, R., Yamasoba, D., Kimura, I., Wang, L., Kishimoto, M., Ito, J., Morioka, Y., Nao, N., Nasser, H., Uriu, K., et al. (2022). Attenuated fusogenicity and pathogenicity of SARS-CoV-2 Omicron variant. Nature *603*, 700–705.
19. Iketani, S., Liu, L., Guo, Y., Liu, L., Chan, J.F.W., Huang, Y., Wang, M., Luo, Y., Yu, J., Chu, H., et al. (2022). Antibody evasion properties of SARS-CoV-2 Omicron sublineages. Nature *604*, 553–556.
20. Nutalai, R., Zhou, D., Tuekprakhon, A., Ginn, H.M., Supasa, P., Liu, C., Huo, J., Mentzer, A.J., Duyvesteyn, H.M.E., Dijokaite-Guraliuc, A., et al. (2022). Potent cross-reactive antibodies following Omicron breakthrough in vaccinees. Cell *185*, 2116–2131.e18.
21. Del Rio, C., and Malani, P.N. (2022). COVID-19 in 2022-the beginning of the end or the end of the beginning? JAMA *327*, 2389–2390.
22. Di Genova, C., Sampson, A., Scott, S., Cantoni, D., Mayora-Neto, M., Bentley, E., Mattiuzzo, G., Wright, E., Derveni, M., Auld, B., et al. (2020). Production, Titration, Neutralisation and Storage of SARS-CoV-2 Lentiviral Pseudotypes (figshare).
23. Flaxman, A., Marchevsky, N.G., Jenkin, D., Aboagye, J., Aley, P.K., Angus, B., Belij-Rammerstorfer, S., Bibi, S., Bittaye, M., Cappuccini, F., et al. (2021). Reactogenicity and immunogenicity after a late second dose or a third dose of ChAdOx1 nCoV-19 in the UK: a substudy of two randomised controlled trials (COV001 and COV002). Lancet *398*, 981–990.
24. Cele, S., Jackson, L., Khoury, D.S., Khan, K., Moyo-Gwete, T., Tegally, H., San, J.E., Cromer, D., Scheepers, C., Amoako, D.G., et al. (2022). Omicron

extensively but incompletely escapes Pfizer BNT162b2 neutralization. Nature *602*, 654–656.

25. Weinreich, D.M., Sivapalasingam, S., Norton, T., Ali, S., Gao, H., Bhore, R., Musser, B.J., Soo, Y., Rofail, D., Im, J., et al. (2021). REGN-COV2, a neutralizing antibody cocktail, in outpatients with covid-19. N. Engl. J. Med. *384*, 238–251.
26. Dong, J., Zost, S.J., Greaney, A.J., Starr, T.N., Dingens, A.S., Chen, E.C., Chen, R.E., Case, J.B., Sutton, R.E., Gilchuk, P., et al. (2021). Genetic and structural basis for SARS-CoV-2 variant neutralization by a two-antibody cocktail. Nat. Microbiol. *6*, 1233–1244.
27. Sun, Y., and Ho, M. (2020). Emerging antibody-based therapeutics against SARS-CoV-2 during the global pandemic. Antib. Ther. *3*, 246–256.
28. Westendorf, K., Žentelis, S., Wang, L., Foster, D., Vaillancourt, P., Wiggin, M., Lovett, E., van der Lee, R., Hendle, J., Pustilnik, A., et al. (2022). LY-CoV1404 (bebtelovimab) potently neutralizes SARS-CoV-2 variants. Cell Rep. *39*, 110812.
29. Xie, X., Liu, Y., Liu, J., Zhang, X., Zou, J., Fontes-Garfias, C.R., Xia, H., Swanson, K.A., Cutler, M., Cooper, D., et al. (2021). Neutralization of SARS-CoV-2 spike 69/70 deletion, E484K and N501Y variants by BNT162b2 vaccine-elicited sera. Nat. Med. *27*, 620–621.
30. Liu, Y., Liu, J., Plante, K.S., Plante, J.A., Xie, X., Zhang, X., Ku, Z., An, Z., Scharton, D., Schindewolf, C., et al. (2022). The N501Y spike substitution enhances SARS-CoV-2 infection and transmission. Nature *602*, 294–299.
31. Cui, Z., Liu, P., Wang, N., Wang, L., Fan, K., Zhu, Q., Wang, K., Chen, R., Feng, R., Jia, Z., et al. (2022). Structural and functional characterizations of infectivity and immune evasion of SARS-CoV-2 Omicron. Cell *185*, 860–871.e13.
32. Hui, K.P.Y., Ho, J.C.W., Cheung, M.C., Ng, K.C., Ching, R.H.H., Lai, K.L., Kam, T.T., Gu, H., Sit, K.Y., Hsin, M.K.Y., et al. (2022). SARS-CoV-2 Omicron variant replication in human bronchus and lung ex vivo. Nature *603*, 715–720.
33. Meng, B., Abdullahi, A., Ferreira, I.A.T.M., Goonawardane, N., Saito, A., Kimura, I., Yamasoba, D., Gerber, P.P., Fatihi, S., Rathore, S., et al. (2022). Altered TMPRSS2 usage by SARS-CoV-2 Omicron impacts infectivity and fusogenicity. Nature *603*, 706–714.
34. Aricescu, A.R., Lu, W., and Jones, E.Y. (2006). A time- and cost-efficient system for high-level protein production in mammalian cells. Acta Crystallogr. D Biol. Crystallogr. *62*, 1243–1250.
35. Stewart, S.A., Dykxhoorn, D.M., Palliser, D., Mizuno, H., Yu, E.Y., An, D.S., Sabatini, D.M., Chen, I.S.Y., Hahn, W.C., Sharp, P.A., et al. (2003). Lentivirus-delivered stable gene silencing by RNAi in primary cells. RNA *9*, 493–501.
36. Nettleship, J.E., Ren, J., Rahman, N., Berrow, N.S., Hatherley, D., Barclay, A.N., and Owens, R.J. (2008). A pipeline for the production of antibody fragments for structural studies using transient expression in HEK 293T cells. Protein Expr. Purif. *62*, 83–89.
37. Emsley, P., Lohkamp, B., Scott, W.G., and Cowtan, K. (2010). Features and development of coot. Acta Crystallogr. D Biol. Crystallogr. *66*, 486–501.
38. Winter, G., Waterman, D.G., Parkhurst, J.M., Brewster, A.S., Gildea, R.J., Gerstel, M., Fuentes-Montero, L., Vollmar, M., Michels-Clark, T., Young, I.D., et al. (2018). DIALS: implementation and evaluation of a new integration package. Acta Crystallogr. D Struct. Biol. *74*, 85–97.
39. Liebschner, D., Afonine, P.V., Baker, M.L., Bunkóczi, G., Chen, V.B., Croll, T.I., Hintze, B., Hung, L.W., Jain, S., McCoy, A.J., et al. (2019). Macromolecular structure determination using X-rays, neutrons and electrons: recent developments in Phenix. Acta Crystallogr. D Struct. Biol. *75*, 861–877.
40. Delano, W.L. (2004). The PyMOL Molecular Graphics System (DeLano Scientific). http://pymol.sourceforge.net/.
41. Folegatti, P.M., Ewer, K.J., Aley, P.K., Angus, B., Becker, S., Belij-Rammerstorfer, S., Bellamy, D., Bibi, S., Bittaye, M., Clutterbuck, E.A., et al. (2020). Safety and immunogenicity of the ChAdOx1 nCoV-19 vaccine against SARS-CoV-2: a preliminary report of a phase 1/2, single-blind, randomised controlled trial. Lancet *396*, 467–478.
42. Nie, J., Li, Q., Wu, J., Zhao, C., Hao, H., Liu, H., Zhang, L., Nie, L., Qin, H., Wang, M., et al. (2020). Establishment and validation of a pseudovirus neutralization assay for SARS-CoV-2. Emerg. Microbes Infect. *9*, 680–686.
43. Huo, J., Le Bas, A., Ruza, R.R., Duyvesteyn, H.M.E., Mikolajek, H., Malinauskas, T., Tan, T.K., Rijal, P., Dumoux, M., Ward, P.N., et al. (2020). Neutralizing nanobodies bind SARS-CoV-2 spike RBD and block interaction with ACE2. Nat. Struct. Mol. Biol. *27*, 846–854.
44. Walter, T.S., Diprose, J., Brown, J., Pickford, M., Owens, R.J., Stuart, D.I., and Harlos, K. (2003). A procedure for setting up high-throughput nanolitre crystallization experiments. I. Protocol design and validation. J. Appl. Cryst. *36*, 308–314.
45. Winter, G. (2010). xia2: an expert system for macromolecular crystallography data reduction. J. Appl. Cryst. *43*, 186–190.
46. Stuart, D.I., Levine, M., Muirhead, H., and Stammers, D.K. (1979). Crystal structure of cat muscle pyruvate kinase at a resolution of 2.6 A. J. Mol. Biol. *134*, 109–142.

STAR★METHODS

KEY RESOURCES TABLE

REAGENT or RESOURCE	SOURCE	IDENTIFIER
Antibodies		
Fab	Dejnirattisai et al.[17]	N/A
IgG	Dejnirattisai et al. and Liu et al.[14,17]	N/A
Human anti-NP (mAb 206)	Dejnirattisai et al.[17]	N/A
Regeneron mAbs	AstraZeneca	Cat#REGN10933 and REGN10987
AstraZeneca mAbs	AstraZeneca	Cat#AZD1061, AZD8895 and AZD7442
Vir mAbs	Adagio	Cat#S309
Lilly mAbs	Adagio	Cat#LY-CoV555, LY-CoV16 and LY-CoV1404
Adagio mAbs	Adagio	Cat#ADG10, ADG20 and ADG30
Omicron antibodies	Nutalai et al.[20]	N/A
Bacterial, Virus Strains, and Yeast	N/A	N/A
DH5α bacteria	In Vitrogen	Cat#18263012
Biological samples		
Serum from Pfizer-vaccinated individuals	University of Oxford	N/A
Serum from AstraZeneca-Oxford-vaccinated individuals	University of Oxford	N/A
Plasma from SARS-CoV-2 patients	John Radcliffe Hospital in Oxford UK, South Africa, and FIOCRUZ (WHO) Brazil	N/A
Chemicals, peptides, and recombinant proteins		
His-tagged SARS-CoV-2 RBD	Dejnirattisai et al.[17]	N/A
His-tagged Avi-tagged SARS-CoV-2/BA.2.75 RBD	This paper	N/A
His-tagged SARS-CoV-2/BA.2 + R493Q RBD	This paper	N/A
His-tagged SARS-CoV-2/BA.2 RBD	Nutalai et al.[20]	N/A
His-tagged SARS-CoV-2/BA.4/5 RBD	Tuekprakhon et al.[12]	N/A
His-tagged SARS-CoV-2/Alpha RBD	Supasa et al.[13]	N/A
Human ACE2-hIgG1Fc	Liu et al.[14]	N/A
Phosphate buffered saline tablets	Sigma-Aldrich	Cat#P4417
Dulbecco's Modified Eagle Medium, high glucose	Sigma-Aldrich	Cat#D5796
Dulbecco's Modified Eagle Medium, low glucose	Sigma-Aldrich	Cat#D6046
FreeStyle™ 293 Expression Medium	Gibco	Cat#12338018
L-Glutamine–Penicillin–Streptomycin solution	Sigma-Aldrich	Cat#G1146
GlutaMAX™ Supplement	Gibco	Cat#35050061
UltraDOMA PF Protein-free Medium	Lonza	Cat#12-727F
Opti-MEM™	Gibco	Cat#11058021
Fetal Bovine Serum	Gibco	Cat#12676029
Strep-Tactin®XT	IBA Lifesciences	Cat#2-1206-025
HEPES	Melford	Cat#34587-39108
LB broth	Fisher Scientific UK	Cat#51577-51656
Trypsin-EDTA	Gibco	Cat#2259288
TrypLE™ Express Enzyme	Gibco	Cat#12604013

(*Continued on next page*)

Continued

REAGENT or RESOURCE	SOURCE	IDENTIFIER
L-Glutamine 200 mM (100X)	Gibco	Cat#2036885
Isopropyl β-d-1-thiogalactopyranoside	Meridian Bioscience	Cat#BIO-37036
Kanamycin	Melford	Cat#K22000
Ampicillin	Sigma-Aldrich	Cat#PHR2838
Agarose	Sigma-Aldrich	Cat#A2929
SYBR™ Safe DNA Gel Stain	Fisher Scientific UK	Cat#S33102
QIAprep Spin Miniprep Kit	Qiagen	Cat#27106X4
QIAquick® PCR & Gel Cleanup Kit	Qiagen	Cat#28704
Phusion™ High-Fidelity DNA Polymerase	Fisher Scientific UK	Cat#F530S
Bright-Glo™ Luciferase Assay System	Promega	Cat#E2620
HIV1 p24 ELISA Kit	Abcam	Cat#ab218268
NaCl	Sigma-Aldrich	Cat#S9888
Sensor Chip Protein A	Cytiva	Cat#29127555
Biotin CAPture Kit, Series S	Cytiva	CAT#28920234
HBS-EP + Buffer 10×	Cytiva	Cat# BR100669
Regeneration Solution (glycine-HCl pH 1.7)	Cytiva	Cat# BR100838
Deposited data		
Crystal structures of SARS-CoV-2 Omicron BA.2.75 RBD in complex with ACE2	This paper	PDB: 8ASY
Experimental models: Cell lines		
HEK293 cells	ATCC	Cat#CRL-3216
Expi293F™ Cells	Gibco,	Cat#A14527
HEK293T/17 cells	ATCC	Cat#CRL-11268™
HEK293T cells	ATCC	Cat#CRL-11268
Vero CCL-81 cells	ATCC	Cat#CCL-81
VeroE6/TMPRSS2 cells	NIBSC	Ref. no. 100978
Recombinant DNA		
Vector: pHLsec	Aricescu et al.[34]	N/A
Vector: pNEO	Aricescu et al.[34]	N/A
Vector: pHLsec-SARS-CoV-2 spike of Omicron	Nutalai et al.[20]	N/A
Vector: pOPINTTGneo-BAP-SARS-CoV-2 RBD of BA.2.75	This paper	N/A
Vector: pNEO-SARS-CoV-2 RBD of BA.2	Nutalai et al.[20]	N/A
Vector: pNEO-SARS-CoV-2 RBD of BA.4/5	Tuekprakhon et al.[12]	N/A
Vector: pNEO-SARS-CoV-2 RBD of BA.2 + R493Q	This paper	N/A
Vector: pNEO-SARS-CoV-2 RBD of Alpha	Supasa et al.[13]	N/A
Vector: pCMV-VSV-G	Stewart et al.[35]	Addgene plasmid # 8454
pHR-SIN-ACE2	Alain Townsend, Oxford	N/A
Vector: pOPING-ET	Nettleship et al.[36]	N/A
Vector: pcDNA-SARS-CoV-2 spike of Victoria strain (S247R)	Liu et al.[14]	N/A
Vector: pcDNA-SARS-CoV-2 spike of BA.1 strain (A67V, Δ69–70, T95I, G142D/Δ143-145, Δ211/L212I, ins214EPE, G339D, S371L, S373P, S375F, K417N, N440K, G446S, S477N, T478K, E484A, Q493R, G496S, Q498R, N501Y, Y505H, T547K, D614G, H655Y, N679K, P681H, N764K, D796Y, N856K, Q954H, N969K, L981F)	Nutalai et al.[20]	N/A

(*Continued on next page*)

Continued

REAGENT or RESOURCE	SOURCE	IDENTIFIER
Vector: pcDNA-SARS-CoV-2 spike of BA.1.1 strain (A67V, Δ69–70, T95I, G142D/ Δ143-145, Δ211/L212I, ins214EPE, G339D, R346K, S371L, S373P, S375F, K417N, N440K, G446S, S477N, T478K, E484A, Q493R, G496S, Q498R, N501Y, Y505H, T547K, D614G, H655Y, N679K, P681H, N764K, D796Y, N856K, Q954H, N969K, L981F)	Nutalai et al.[20]	N/A
Vector: pcDNA-SARS-CoV-2 spike of BA.2 strain (T19I, Δ24–26, A27S, G142D, V213G, G339D, S371F, S373P, S375F, T376A, D405N, R408S, K417N, N440K, S477N, T478K, E484A, Q493R, Q498R, N501Y, Y505H, D614G, H655Y, N679K, P681H, N764K, D796Y, Q954H, N969K)	Nutalai et al.[20]	N/A
Vector: pcDNA-SARS-CoV-2 spike of BA.2.12.1 strain (T19I, Δ24–26, A27S, G142D, V213G, G339D, S371F, S373P, S375F, T376A, D405N, R408S, K417N, N440K, L452Q, S477N, T478K, E484A, Q493R, Q498R, N501Y, Y505H, D614G, H655Y N679K, P681H, S704L, N764K, D796Y, Q954H, N969K)	Nutalai et al.[20]	N/A
Vector: pcDNA-SARS-CoV-2 spike of BA.4/5 strain (T19I, Δ24–26, A27S, Δ69-70, G142D, V213G, G339D, S371F, S373P, S375F, T376A, D405N, R408S, K417N, N440K, L452R, S477N, T478K, E484A, F486V, Q498R, N501Y, Y505H, D614G, H655Y, N679K, P681H, N764K, D796Y, Q954H, N969K)	Tuekprakhon et al.[12]	N/A
Vector: pcDNA-SARS-CoV-2 spike of BA.2.75 strain (T19I, Δ24–26, A27S, G142D, K147E, W152R, F157L, I210V, V213G, G257S, D339H, S371F, S373P, S375F, T376A, D405N, R408S, K417N, N440K, G446S, N460K, S477N, T478K, E484A, R493Q, Q498R, N501Y, Y505H, D614G, H655Y, N679K, P681H, N764K, D796Y, Q954H, N969K)	This paper	N/A
Vector: pcDNA-SARS-CoV-2 spike of BA.2 + D339H strain (T19I, Δ24–26, A27S, G142D, V213G, D339H, S371F, S373P, S375F, T376A, D405N, R408S, K417N, N440K, S477N, T478K, E484A, Q493R, Q498R, N501Y, Y505H, D614G, H655Y, N679K, P681H, N764K, D796Y, Q954H, N969K)	This paper	N/A
Vector: pcDNA-SARS-CoV-2 spike of BA.2 + R493Q strain (T19I, Δ24–26, A27S, G142D, V213G, G339D, S371F, S373P, S375F, T376A, D405N, R408S, K417N, N440K, S477N, T478K, E484A, R493Q, Q498R, N501Y, Y505H, D614G, H655Y, N679K, P681H, N764K, D796Y, Q954H, N969K)	This paper	N/A
Vector: pcDNA-SARS-CoV-2 spike of BA.2 + G446S strain (T19I, Δ24–26, A27S, G142D, V213G, G339D, S371F, S373P, S375F, T376A, D405N, R408S, K417N, N440K, G446S, S477N, T478K, E484A, Q493R, Q498R, N501Y, Y505H, D614G, H655Y, N679K, P681H, N764K, D796Y, Q954H, N969K)	This paper	N/A

(*Continued on next page*)

Continued

REAGENT or RESOURCE	SOURCE	IDENTIFIER
Vector: human IgG1 heavy chain	German Cancer Research Center, Heidelberg, Germany (H. Wardemann	N/A
Vector: human lambda light chain	German Cancer Research Center, Heidelberg, Germany (H. Wardemann	N/A
Vector: human kappa light chain	German Cancer Research Center, Heidelberg, Germany (H. Wardemann	N/A
Vector: Human Fab	Univeristy of Oxford	N/A
Vector: pJYDC1	Adgene	ID: 162,458
TM149 BirA pDisplay	University of Oxford, NDM (C. Siebold)	N/A
Software and algorithms		
COOT	Emsley et al.[37]	https://www2.mrc-lmb.cam.ac.uk/personal/pemsley/coot/
Xia2-dials	Winter et al.[38]	https://xia2.github.io/parameters.html
PHENIX	Liebschner et al.[39]	https://www.phenix-online.org/
PyMOL	Warren DeLano,[40]	https://pymol.org/
Data Acquisition Software 11.1.0.11	Fortebio	https://www.fortebio.com/products/octet-systems-software
Data Analysis Software HT 11.1.0.25	Fortebio	https://www.fortebio.com/products/octet-systems-software
Prism 9.0	GraphPad	https://www.graphpad.com/scientific-software/prism/
Yeast display titration curve fitting were done by the standard non-cooperative Hill equation, fitted by nonlinear least-squares regression with two additional parameters using Python 3.7	Zahradnik et al.[11]	N/A
IBM SPSS Software 27	IBM	https://www.ibm.com
Mabscape	This paper	https://github.com/helenginn/mabscape https://snapcraft.io/mabscape
Biacore T200 Evaluation Software 3.1	Cytiva	www.cytivalifesciences.com
Other		
X-ray data were collected at beamline I03, Diamond Light Source, under proposal ib27009 for COVID-19 rapid access	This paper	https://www.diamond.ac.uk/covid-19/for-scientists/rapid-access.html
TALON® Superflow Metal Affinity Resin	Clontech	Cat#635668
HiLoad® 16/600 Superdex® 200 pg	Cytiva	Cat#28-9893-35
Superdex 200 increase 10/300 GL column	Cytiva	Cat#28990944
HisTrap nickel HP 5-mL column	Cytiva	Cat#17524802
HiTrap Heparin HT 5-mL column	Cytiva	Cat#17040703
Amine Reactive Second-Generation (AR2G) Biosensors	Fortebio	Cat#18-5092
Octet RED96e	Fortebio	https://www.fortebio.com/products/label-free-bli-detection/8-channel-octet-systems
Buffer exchange system "QuixStand"	GE Healthcare	Cat#56-4107-78
Cartesian dispensing system	Genomic solutions	Cat#MIC4000

(*Continued on next page*)

Continued

REAGENT or RESOURCE	SOURCE	IDENTIFIER
Hydra-96	Robbins Scientific	Cat#Hydra-96
96-well crystallization plate	Greiner bio-one	Cat#E20113NN
Crystallization Imaging System	Formulatrix	Cat#RI-1000
Sonics vibra-cell vcx500 sonicator	VWR	Cat#432-0137
Biacore T200	Cytiva	https://www.cytivalifesciences.com/en/us/shop/protein-analysis/spr-label-free-analysis/systems/biacore-t200-p-05644

RESOURCE AVAILABILITY

Lead contact

Further information and requests for resources and reagents should be directed to and will be fulfilled by the lead contact, David I Stuart (dave@strubi.ox.ac.uk).

Materials availability

Reagents generated in this study are available from the lead contact with a completed Materials Transfer Agreement.

Data and code availability

- Data availability. The coordinates and structure factors of the crystallographic complex are available from the PDB with accession code 8ASY.
- Code availability. This paper does not report original code.
- Reagents generated in this study are available from the lead contact with a completed Materials Transfer Agreement. Any additional information required to reanalyze the data reported in this paper is available from the lead contact upon request.

EXPERIMENTAL MODEL AND SUBJECT DETAILS

Bacterial strains and cell culture

Vero (ATCC CCL-81) and VeroE6/TMPRSS2 cells were cultured at 37°C in Dulbecco's Modified Eagle medium (DMEM) high glucose (Sigma-Aldrich) supplemented with 10% fetal bovine serum (FBS), 2 mM GlutaMAX (Gibco, 35050061) and 100 U/mL of penicillin–streptomycin. Human mAbs were expressed in HEK293T cells cultured in UltraDOMA PF Protein-free Medium (Cat# 12-727F, LONZA) at 37°C with 5% CO_2. HEK293T (ATCC CRL-11268) cells were cultured in DMEM high glucose (Sigma-Aldrich) supplemented with 10% FBS, 1% 100X Mem Neaa (Gibco) and 1% 100X L-Glutamine (Gibco) at 37°C with 5% CO_2. To express RBD, RBD variants and ACE2, HEK293T cells were cultured in DMEM high glucose (Sigma) supplemented with 2% FBS, 1% 100X Mem Neaa and 1% 100X L-Glutamine at 37°C for transfection. Omicron RBD and human mAbs were also expressed in HEK293T (ATCC CRL-11268) cells cultured in FreeStyle 293 Expression Medium (ThermoFisher, 12338018) at 37°C with 5% CO_2. *E.coli DH5*α bacteria were used for transformation and large-scale preparation of plasmids. A single colony was picked and cultured in LB broth at 37 °C at 200 rpm in a shaker overnight.

Plasma from early pandemic and Alpha cases

Participants from the first wave of SARS-CoV2 in the U.K. and those sequence confirmed with B.1.1.7 lineage in December 2020 and February 2021 were recruited through three studies: Sepsis Immunomics [Oxford REC C, ref. 19/SC/0296]), ISARIC/WHO Clinical Characterisation Protocol for Severe Emerging Infections [Oxford REC C, ref. 13/SC/0149] and the Gastro-intestinal illness in Oxford: COVID sub study [Sheffield REC, ref. 16/YH/0247]. Diagnosis was confirmed through reporting of symptoms consistent with COVID-19 and a test positive for SARS-CoV-2 using reverse transcriptase polymerase chain reaction (RT-PCR) from an upper respiratory tract (nose/throat) swab tested in accredited laboratories. A blood sample was taken following consent at least 14 days after symptom onset. Clinical information including severity of disease (mild, severe or critical infection according to recommendations from the World Health Organisation) and times between symptom onset and sampling and age of participant was captured for all individuals at the time of sampling. Following heat inactivation of plasma/serum samples they were aliquoted so that no more than 3 freeze thaw cycles were performed for data generation. For subject details see Table S3.

Sera from BA.4/5 infected cases, study subjects

Following informed consent, individuals with omicron BA.4 or BA.5 were co-enrolled into one or more of the following three studies: the ISARIC/WHO Clinical Characterisation Protocol for Severe Emerging Infections [Oxford REC C, ref. 13/SC/0149], the "Innate and

adaptive immunity against SARS-CoV-2 in healthcare worker family and household members'' protocol (approved by the University of Oxford Central University Research Ethics Committee), or the Gastro-intestinal illness in Oxford: COVID sub study [Sheffield REC, ref. 16/YH/0247]. Diagnosis was confirmed through reporting of symptoms consistent with COVID-19, hospital presentation, and a test positive for SARS-CoV-2 using reverse transcriptase polymerase chain reaction (RT-PCR) from an upper respiratory tract (nose/throat) swab tested in accredited laboratories and lineage sequence confirmed through national reference laboratories in the United Kingdom. A blood sample was taken following consent at least 14 days after PCR test confirmation. Clinical information including severity of disease (mild, severe or critical infection according to recommendations from the World Health Organisation) and times between symptom onset and sampling and age of participant was captured for all individuals at the time of sampling. For subject details see Table S3.

Sera from Beta, Gamma and Delta infected cases

Beta and Delta samples from UK infected cases were collected under the ''Innate and adaptive immunity against SARS-CoV-2 in healthcare worker family and household members'' protocol affiliated to the Gastro-intestinal illness in Oxford: COVID sub study discussed above and approved by the University of Oxford Central University Research Ethics Committee. All individuals had sequence confirmed Beta/Delta infection or PCR-confirmed symptomatic disease occurring whilst in isolation and in direct contact with Beta/Delta sequence-confirmed cases. Additional Beta infected serum (sequence confirmed) was obtained from South Africa. At the time of swab collection patients signed an informed consent to consent for the collection of data and serial blood samples. The study was approved by the Human Research Ethics Committee of the University of the Witwatersrand (reference number 200313) and conducted in accordance with Good Clinical Practice guidelines. Gamma samples were provided by the International Reference Laboratory for Coronavirus at FIOCRUZ (WHO) as part of the national surveillance for coronavirus and had the approval of the FIOCRUZ ethical committee (CEP 4.128.241) to continuously receive and analyze samples of COVID-19 suspected cases for virological surveillance. Clinical samples were shared with Oxford University, UK under the MTA IOC FIOCRUZ 21-02. For subject details see Table S3.

Sera from BA.1 infected cases, study subjects

Following informed consent, individuals with omicron BA.1 were co-enrolled into the ISARIC/WHO Clinical Characterisation Protocol for Severe Emerging Infections [Oxford REC C, ref. 13/SC/0149] and the ''Innate and adaptive immunity against SARS-CoV-2 in healthcare worker family and household members'' protocol affiliated to the Gastro-intestinal illness in Oxford: COVID sub study [Sheffield REC, ref. 16/YH/0247] further approved by the University of Oxford Central University Research Ethics Committee. Diagnosis was confirmed through reporting of symptoms consistent with COVID-19 or a positive contact of a known Omicron case, and a test positive for SARS-CoV-2 using reverse transcriptase polymerase chain reaction (RT-PCR) from an upper respiratory tract (nose/throat) swab tested in accredited laboratories and lineage sequence confirmed through national reference laboratories. A blood sample was taken following consent at least 10 days after PCR test confirmation. Clinical information including severity of disease (mild, severe or critical infection according to recommendations from the World Health Organisation) and times between symptom onset and sampling and age of participant was captured for all individuals at the time of sampling. For subject details see Table S3.

Sera from BA.2 infected cases, study subjects

Following informed consent, healthcare workers with BA.2 infection were co-enrolled under the Sheffield Biobank study (STHObs) (18/YH/0441). All individuals had PCR-confirmed symptomatic disease and sequence confirmed BA.2 infection through national UKHSA sequencing data. A blood sample was taken following consent at least 12 days after PCR test confirmation. Clinical information including vaccination history, times between symptom onset and sampling and age of participant was captured for all individuals at the time of sampling. For subject details see Table S3.

Sera from Pfizer vaccinees

Pfizer vaccine serum was obtained from volunteers who had received three doses of the BNT162b2 vaccine. Vaccinees were Health Care Workers, based at Oxford University Hospitals NHS Foundation Trust, not known to have prior infection with SARS-CoV-2 and were enrolled in the OPTIC Study as part of the Oxford Translational Gastrointestinal Unit GI Biobank Study 16/YH/0247 [research ethics committee (REC) at Yorkshire & The Humber – Sheffield] which has been amended for this purpose on 8 June 2020. The study was conducted according to the principles of the Declaration of Helsinki (2008) and the International Conference on Harmonization (ICH) Good Clinical Practice (GCP) guidelines. Written informed consent was obtained for all participants enrolled in the study. Participants were sampled approximately 28 days (range 25–56) after receiving a third ''booster dose of BNT162B2 vaccine. The mean age of vaccinees was 37 years (range 22–66), 21 male and 35 female.

AstraZeneca-Oxford vaccine study procedures and sample processing

Full details of the randomized controlled trial of ChAdOx1 nCoV-19 (AZD1222), were previously published (PMID: 33220855/PMID: 32702298). These studies were registered at ISRCTN (15281137 and 89951424) and ClinicalTrials.gov (NCT04324606 and NCT04400838). Written informed consent was obtained from all participants, and the trial is being done in accordance with the principles of the Declaration of Helsinki and Good Clinical Practice. The studies were sponsored by the University of Oxford (Oxford, UK) and approval obtained from a national ethics committee (South Central Berkshire Research Ethics Committee, ref. 20/SC/0145 and

20/SC/0179) and a regulatory agency in the United Kingdom (the Medicines and Healthcare Products Regulatory Agency). An independent DSMB reviewed all interim safety reports. A copy of the protocols was included in previous publications.[41] Data from vaccinated volunteers who received three vaccinations are included in this study. Blood samples were collected and serum separated approximately 28 days (range 26–34 days) following the third dose. For subject details see column 'AZ V3+28' in Table S3.

METHOD DETAILS

Pseudovirus plasmid construction and lentiviral particles production

Pseudotyped lentivirus expressing SARS-CoV-2 S proteins from ancestral strain (Victoria, S247R), BA.1, BA.1.1, BA.2 and BA.4/5 were constructed as described previously.[12,14,20,42] We applied the same method to construct BA.2.12.1, and BA.2.75, by adding more mutations into the BA.2 construct. To generate BA.2.75, we added K147E, W152R, F157L, I210V, G275S, G446S and N460K into BA.2 backbone, also changed 339D in BA.2 S into 339H, and reversed 493R in BA.2 to 493Q as in the ancestral strain. To test single mutation impact, we introduced D339H, G446S, N460K and R493Q individually into BA.2 backbone. The resulting pcDNA3.1 plasmid carrying S gene was used for generating pseudoviral particles together with the lentiviral packaging vector and transfer vector encoding luciferase reporter. All the constructs were sequence confirmed.

Pseudoviral neutralization test

The pseudoviral neutralization test has been described previously.[14] Briefly, the neutralizing activity of potent monoclonal antibodies generated from donors who had recovered from BA.1 infection were tested against Victoria, BA.1, BA.1.1, BA.2, BA.3, BA.4/5, BA.2.75 and BA.2 + N460K. Four-fold serial diluted mAbs were incubated with pseudoviral particles at 37°C, 5% CO_2 for 1 h. Stable HEK293T/17 cells expressing human ACE2 were then added to the mixture at 1.5×10^4 cells/well. 48 h post infection, culture supernatants were removed and 50 μL of 1:2 Bright-Glo TM Luciferase assay system (Promega, USA) in 1 × PBS was added to each well. The reaction was incubated at room temperature for 5 min and firefly luciferase activity was measured using CLARIOstar (BMG Labtech, Ortenberg, Germany). The percentage neutralization was calculated relative to the control. Probit analysis was used to estimate the dilution that inhibited half maximum pseudotyped lentivirus infection (PVNT50).

To determine the neutralizing activity of convalescent plasma/serum samples or vaccine sera, 3-fold serial dilutions of each samples were incubated with pseudoviral particles for 1 h and the same strategy as mAb was applied.

Cloning of RBDs

To generate the BA.2.75 RBD construct, site-directed PCR mutagenesis was performed using the BA.2 Spike construct as the template,[20] with the introduction of D339H, G446S, N460K and R493Q mutations using primers listed in Table S4; the gene fragment was amplified with D339H_pNeoF and RBD333_BAP_R (Table S4), and cloned into the pOPINTTGneo-BAP vector.[43] To generate the BA.2 + R493Q RBD construct, site-directed PCR mutagenesis was performed using the BA.2 Spike construct as the template, with the introduction of R493Q mutation suing primers listed in Table S4; the gene fragment was amplified with pNeoRBD333Omi_F and RBD333_BAP_R, and cloned into the pNeo vector.[13] Cloning was performed using the ClonExpress II One Step Cloning Kit (Vazyme). The Constructs were verified by Sanger sequencing after plasmid isolation using QIAGEN Miniprep kit (QIAGEN).

Production of RBDs

Plasmids encoding RBDs were transfected into Expi293F Cells (ThermoFisher) by PEI, cultured in FreeStyle 293 Expression Medium (ThermoFisher) at 37°C for 1 day followed by 30°C for 3 days with 8% CO_2. To express biotinylated RBDs, the RBD-BAP plasmid was co-transfected with pDisplay-BirA-ER (Addgene plasmid 20,856; coding for an ER-localized biotin ligase), in the presence of 0.8 mM D-biotin (Sigma-Aldrich). The conditioned medium was diluted 1:2 into binding buffer (50 mM sodium phosphate, 500 mM sodium chloride, pH 8.0). RBDs were purified with a 5 mL HisTrap nickel column (GE Healthcare) through His-tag binding, followed by a Superdex 75 10/300 GL gel filtration column (GE Healthcare) in 10 mM HEPES and 150 mM sodium chloride.

Surface plasmon resonance

Surface plasmon resonance experiments were performed using a Biacore T200 (GE Healthcare). All assays were performed with running buffer of HBS-EP (Cytiva) at 25°C.

To determine the binding kinetics between BA.2.75 or BA.2 + R493Q RBD and ACE2, a Protein A sensor chip (Cytiva) was used. ACE2-Fc was immobilised onto the sample flow cell of the sensor chip. The reference flow cell was left blank. RBD was injected over the two flow cells at a range of five concentrations prepared by serial two-fold dilutions, at a flow rate of 30 μL min^{-1} using a single-cycle kinetics program. Running buffer was also injected using the same program for background subtraction. All data were fitted to a 1:1 binding model using Biacore T200 Evaluation Software 3.1.

To confirm the binding kinetics between the BA.2.75 RBD and ACE2, a Biotin CAPture Kit (Cytiva) was used. Biotinylated ACE2 (bio-ACE2) was immobilised onto the sample flow cell of the sensor chip. The reference flow cell was left blank. The BA.2.75 RBD was injected over the two flow cells at a range of five concentrations prepared by serial two-fold dilutions, at a flow rate of 30 μL min^{-1} using a single-cycle kinetics program. Running buffer was also injected using the same program for background subtraction. All data were fitted to a 1:1 binding model using Biacore T200 Evaluation Software 3.1.

To determine the binding kinetics between the BA.2.75 or BA.2 RBD and mAbs, a Biotin CAPture Kit (Cytiva) was used. Biotinylated RBD was immobilised onto the sample flow cell of the sensor chip. The reference flow cell was left blank. The Fab of Omi-18 or Omi-32 was injected over the two flow cells at a range of five concentrations prepared by serial two-fold dilutions, at a flow rate of 30 μL min^{-1} using a single-cycle kinetics program. For the binding of Omi-20 for bio-BA.2 RBD, the Fab of Omi-20 was injected over the two flow cells at a range of five concentrations prepared by serial two-fold dilutions, at a flow rate of 30 μL min^{-1} using a single-cycle kinetics program. For the binding of Omi-20 for bio-BA.2.75 RBD, the Fab of Omi-20 was injected over the two flow cells at a range of eight concentrations prepared by serial twofold dilutions, at a flow rate of 30 μL min^{-1}. Running buffer was also injected using the same program for background subtraction. All data were fitted to a 1:1 binding model using Biacore T200 Evaluation Software 3.1.

To compare the binding profiles between BA.2 and BA.2.75 RBD for mAb Omi-29, a Biotin CAPture Kit (Cytiva) was used. Biotinylated BA.2 and BA.2.75 RBD was immobilised onto the sample flow cell of the sensor chip to a similar level (~110 RU). The reference flow cell was left blank. A single injection of mAb Fab was performed over the two flow cells at 1 μM, at a flow rate of 30 μL min^{-1}. Running buffer was also injected using the same program for background subtraction. The sensorgrams were plotted using Prism9 (GraphPad).

To compare the binding profiles between BA.2 and BA.2.75 RBD for mAb Omi-36, a sensor chip Protein A (Cytiva) was used. mAb Omi-36 in the IgG form was immobilised onto the sample flow cell of the sensor chip. The reference flow cell was left blank. A single injection of RBD was performed over the two flow cells at 200 nM, at a flow rate of 30 μL min^{-1}. Running buffer was also injected using the same program for background subtraction. The sensorgrams were plotted using Prism9 (GraphPad).

IgG mAbs and Fabs production

AstraZeneca and Regeneron antibodies were provided by AstraZeneca, Vir, Lilly and Adagio antibodies were provided by Adagio, LY-CoV1404 was provided by LifeArc. For the in-house antibodies, heavy and light chains of the indicated antibodies were transiently transfected into 293T cells and antibody purified from supernatant on protein A as previously described.[20] Fabs were digested from purified IgGs with papain using a Pierce Fab Preparation Kit (Thermo Fisher), following the manufacturer's protocol.

Crystallization, X-Ray data collection and structure determination

Purified BA.2.75 RBD was deglycosylated with Endoglycosidase H1 and mixed with ACE2 in a 1:1 M ratio, with a final concentration of 13.0 mg mL^{-1}. Initial screening of crystals was set up in Crystalquick 96-well X plates (Greiner Bio-One) with a Cartesian Robot using the nanoliter sitting-drop vapor-diffusion method, with 100 nL of protein plus 100 nL of reservoir in each drop, as previously described.[44] Crystals of BA.2.75 RBD-ACE2 complex were formed in Hampton Research PEGRx condition 2–25, containing 0.1% (w/v) n-Octyl-b-D-glucoside, 0.1 M Sodium citrate tribasic dihydrate pH 5.5 and 22% (w/v) PEG 3350. Crystals were mounted in loops and dipped in solution containing 25% glycerol and 75% mother liquor for a second before frozen in liquid nitrogen. Diffraction data were collected at 100 K at beamline I03 of Diamond Light Source, UK, using the automated queue system that allows unattended automated data collection (https://www.diamond.ac.uk/Instruments/Mx/I03/I03-Manual/Unattended-Data-Collections.html). The best crystal diffracted to 2.85 Å resolution. 3600 diffraction images of 0.1° each were collected and automatically processed with Xia2-dials.[38,45] The structure was determined by rigid body refinement using the model of BA.2 RBD/ACE2 complex (PDB, 7ZF7)[20] of which the unit cell is isomorphous to the current crystal. Model rebuilding is done with COOT[37] and refinement with Phenix.[39]

Data collection and structure refinement statistics are given in Table S5. Structural comparisons used SHP[46] and figures were prepared with PyMOL (The PyMOL Molecular Graphics System, Version 1.2r3pre, Schrödinger, LLC).

Antigenic mapping

Antigenic mapping of omicron was carried out using a previously described.[12] In short, coronavirus variants were assigned three-dimensional coordinates whereby the distance between two points indicates the base drop in neutralization titer. Each serum was assigned a strength parameter which provided a scalar offset to the logarithm of the neutralization titer. These parameters were refined to match predicted neutralization titers to observed values by taking an average of superimposed positions from 30 separate runs. The three-dimensional positions of the variants of concern: Victoria, Alpha, Beta, Gamma, Delta and Omicron were plotted for display.

QUANTIFICATION AND STATISTICAL ANALYSIS

Statistical analyses are reported in the results and figure legends. Neutralization was measured on pseudovirus. The percentage reduction was calculated and IC_{50} determined using the probit program from the SPSS package. The Wilcoxon matched-pairs signed rank test was used for the analysis and two-tailed p values were calculated on geometric mean values.

Cell Reports, Volume *42*

Supplemental information

A delicate balance between antibody evasion and ACE2 affinity for Omicron BA.2.75

Jiandong Huo, Aiste Dijokaite-Guraliuc, Chang Liu, Daming Zhou, Helen M. Ginn, Raksha Das, Piyada Supasa, Muneeswaran Selvaraj, Rungtiwa Nutalai, Aekkachai Tuekprakhon, Helen M.E. Duyvesteyn, Alexander J. Mentzer, Donal Skelly, Thomas G. Ritter, Ali Amini, Sagida Bibi, Sandra Adele, Sile Ann Johnson, Neil G. Paterson, Mark A. Williams, David R. Hall, Megan Plowright, Thomas A.H. Newman, Hailey Hornsby, Thushan I. de Silva, Nigel Temperton, Paul Klenerman, Eleanor Barnes, Susanna J. Dunachie, Andrew J. Pollard, Teresa Lambe, Philip Goulder, OPTIC consortium, ISARIC4C consortium, Elizabeth E. Fry, Juthathip Mongkolsapaya, Jingshan Ren, David I. Stuart, and Gavin R. Screaton

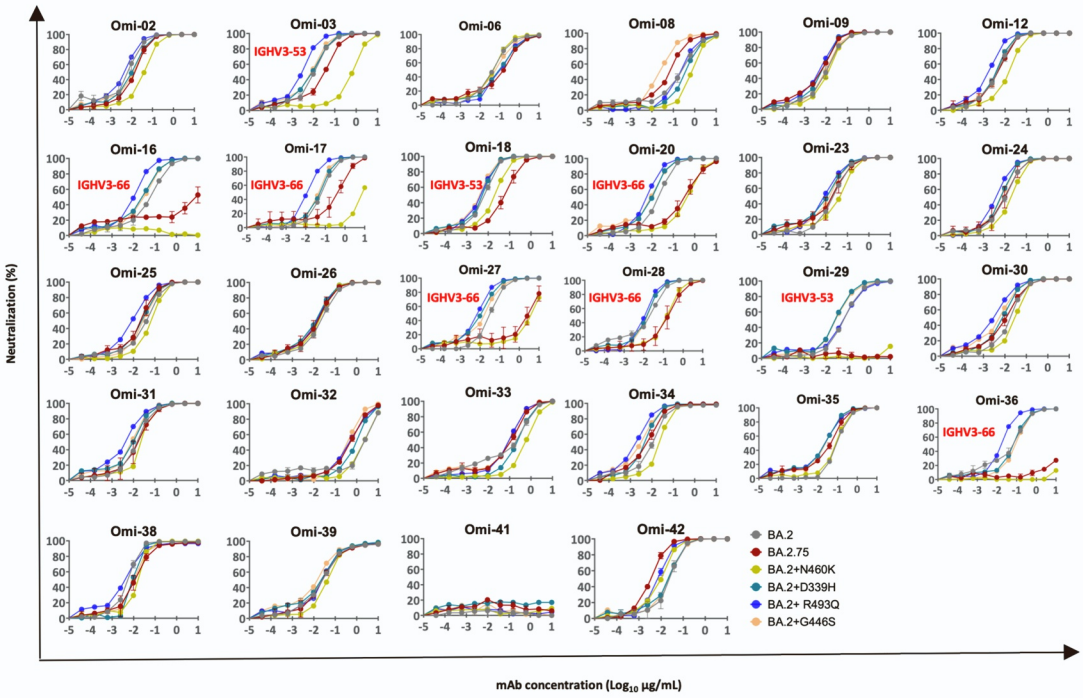

Figure S1 Pseudoviral neutralization assays against monoclonal antibodies. (A) Neutralization curves for a panel of 28 monoclonal antibodies made from samples taken from vaccinees infected with BA.1. Titration curves for single mutations of BA.2.27 in the BA.2 background are compared with BA.2 and BA.2.75. IC50 titres are shown in Table S2. Related to Figure 5. All assays have been done at least twice.

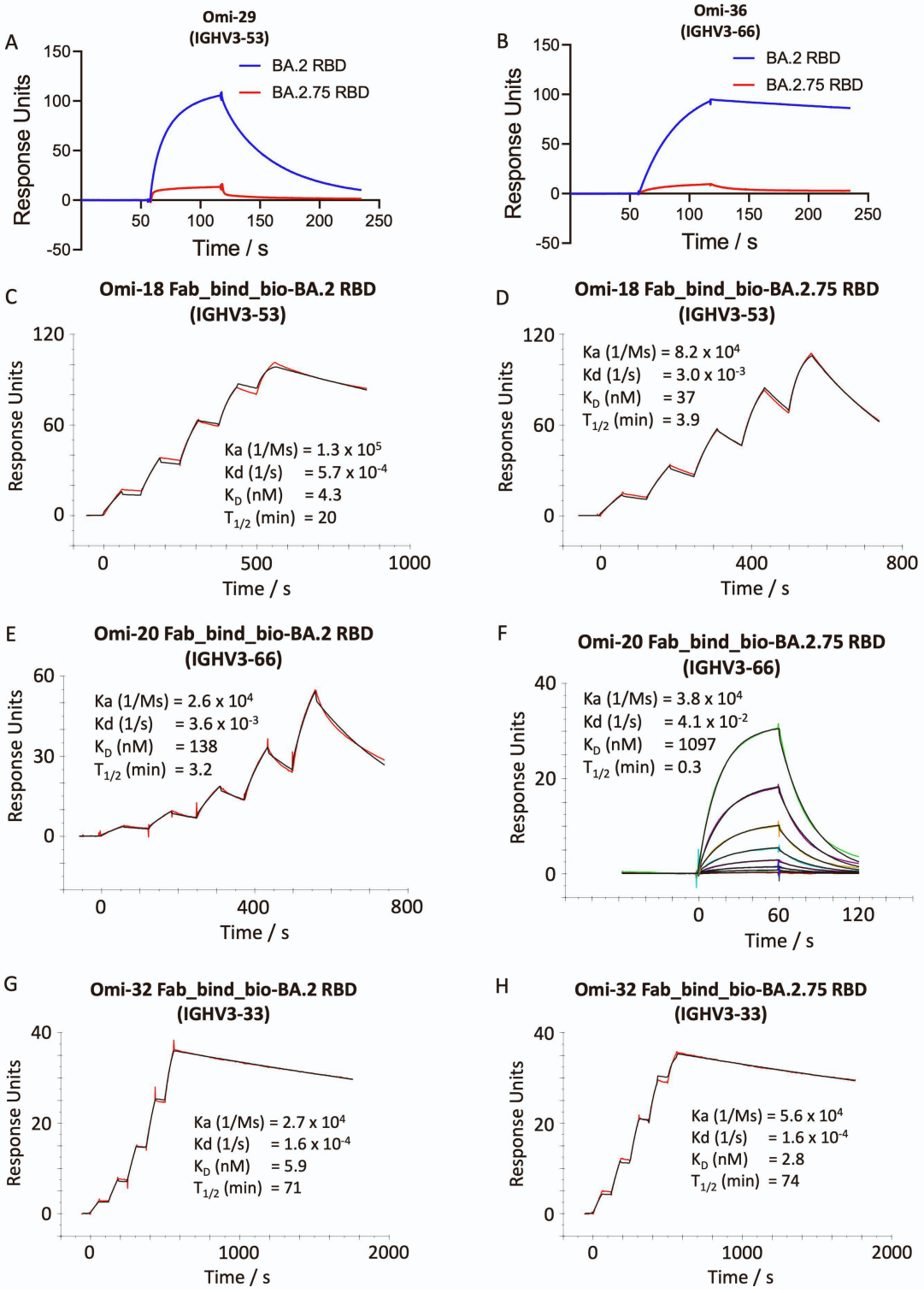

Figure S2 Surface plasmon resonance (SPR) analysis of interaction between BA.2 or BA.2.75 RBD and selected mAbs. (A) Binding of Omi-29 (IGHV3-53) to BA.2.75 RBD is severely reduced compared to that of BA.2, as shown by a single-injection of 1 μM Omi-29 Fab over sample flow cells containing biotinylated BA.2 or BA.2.75 RBD. (B) Binding of Omi-36 (IGHV3-66) to BA.2.75 RBD is severely reduced compared to that of BA.2, as shown by a single-injection of 0.2 μM BA.2 or BA.2.75 RBD over sample flow cells containing Omi-36 in the IgG form. (C-H) Sensorgrams (Red / Coloured: original binding curve; black: fitted curve) showing the interactions between BA.2 or BA.4/5 RBD and selected mAbs, with kinetics data shown. Related to Figure 5.

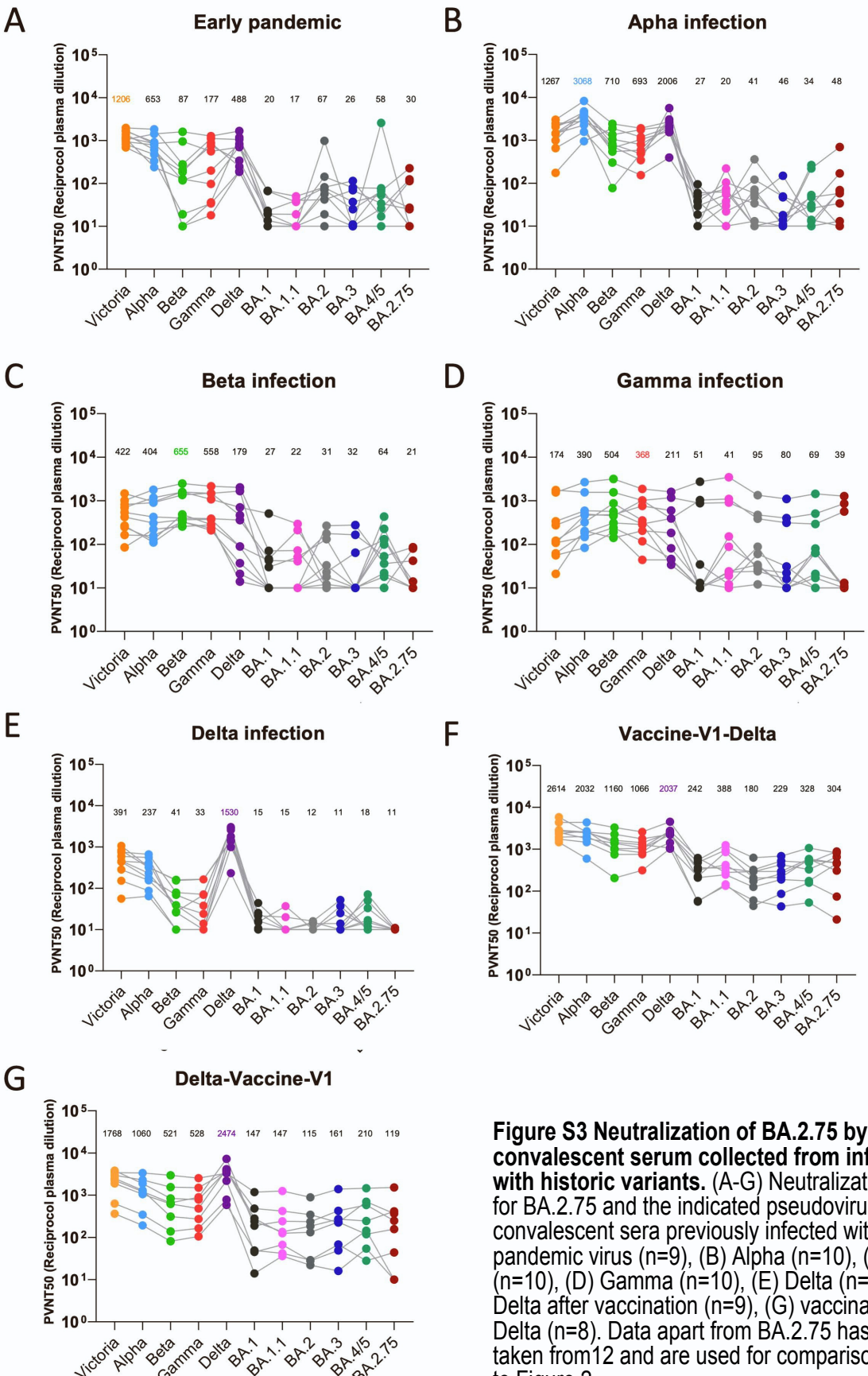

Figure S3 Neutralization of BA.2.75 by panels of convalescent serum collected from infection with historic variants. (A-G) Neutralization titres for BA.2.75 and the indicated pseudoviruses using convalescent sera previously infected with (A) Early pandemic virus (n=9), (B) Alpha (n=10), (C) Beta (n=10), (D) Gamma (n=10), (E) Delta (n=10), (F) Delta after vaccination (n=9), (G) vaccination after Delta (n=8). Data apart from BA.2.75 has been taken from12 and are used for comparison. Related to Figure 2.

Figure S3

Table S1. (A) IC50 of BA.1 mAbs against Victoria and Omicron variant PV including BA.2.75 and BA.2+N460K (related to Figure 5A)

mAbs	Victoria	BA.1	BA.1.1	BA.2	BA.3	BA.4/5	BA.2.75	BA.2+N460K
Omi-02	0.002 ± 0.001	0.004 ± 0.001	0.004 ± 0.001	0.003 ± 0.001	0.019 ± 0.007	>10	0.009 ± 0.002	0.025 ± 0.003
Omi-03 (3-53)	0.003 ± 0.000	0.005 ± 0.002	0.003 ± 0.001	0.008 ± 0.001	0.022 ± 0.003	0.017 ± 0.005	0.017 ± 0.000	0.401 ± 0.026
Omi-06	0.007 ± 0.000	0.017 ± 0.003	0.139 ± 0.033	0.039 ± 0.008	0.696 ± 0.106	>10	0.063 ± 0.005	0.026 ± 0.002
Omi-08	0.008 ± 0.004	0.003 ± 0.000	0.002 ± 0.000	0.114 ± 0.045	0.032 ± 0.001	0.086 ± 0.005	0.036 ± 0.002	0.552 ± 0.090
Omi-09	0.006 ± 0.002	0.005 ± 0.000	0.005 ± 0.002	0.008 ± 0.002	0.017 ± 0.002	0.166 ± 0.007	0.003 ± 0.000	0.010 ± 0.002
Omi-12	0.006 ± 0.002	0.002 ± 0.000	0.002 ± 0.001	0.003 ± 0.001	0.006 ± 0.001	0.429 ± 0.060	0.003 ± 0.001	0.011 ± 0.002
Omi-16 (3-66)	0.014 ± 0.003	0.012 ± 0.002	0.011 ± 0.003	0.034 ± 0.012	0.111 ± 0.008	0.029 ± 0.007	>10	>10
Omi-17 (3-66)	0.023 ± 0.011	0.018 ± 0.012	0.022 ± 0.009	0.060 ± 0.004	0.123 ± 0.002	0.028 ± 0.001	0.255 ± 0.169	>10
Omi-18 (3-53)	0.008 ± 0.003	0.002 ± 0.000	0.002 ± 0.000	0.005 ± 0.000	0.006 ± 0.002	0.005 ± 0.001	0.035 ± 0.007	0.014 ± 0.002
Omi-20 (3-66)	0.009 ± 0.002	0.006 ± 0.001	0.005 ± 0.001	0.015 ± 0.003	0.020 ± 0.004	0.014 ± 0.006	0.178 ± 0.075	0.315 ± 0.142
Omi-23	0.005 ± 0.002	0.029 ± 0.006	0.023 ± 0.12	0.019 ± 0.005	0.011 ± 0.000	>10	0.011 ± 0.006	0.022 ± 0.005
Omi-24	0.005 ±0.000	0.006 ± 0.002	0.054 ± 0.015	0.007 ± 0.001	0.009 ± 0.002	>10	0.008 ± 0.004	0.014 ± 0.000
Omi-25	0.005 ± 0.001	0.023 ± 0.005	0.027 ± 0.005	0.024 ± 0.004	0.050 ± 0.004	>10	0.014 ± 0.005	0.050 ± 0.010
Omi-26	0.002 ± 0.001	0.006 ± 0.002	0.005 ± 0.001	0.013 ± 0.001	0.018 ± 0.002	>10	0.010 ± 0.004	0.010 ± 0.000
Omi-27 (3-66)	0.008 ± 0.003	0.026 ± 0.006	0.034 ± 0.009	0.034 ± 0.005	0.026 ± 0.007	0.069 ± 0.023	6.672 ± 4.466	>10
Omi-28 (3-66)	0.022 ± 0.000	0.011 ± 0.004	0.009 ± 0.002	0.008 ± 0.000	0.019± 0.000	0.028 ± 0.009	0.133 ± 0.082	0.103 ± 0.048
Omi-29 (3-53)	0.014 ± 0.006	0.017 ± 0.003	0.016 ± 0.009	0.056 ± 0.014	0.064 ± 0.017	0.396 ± 0.007	>10	>10
Omi-30	0.012 ± 0.002	0.008 ± 0.003	0.008 ± 0.004	0.011 ± 0.002	0.015 ± 0.003	>10	0.008 ± 0.002	0.018 ± 0.001
Omi-31	0.376± 0.090	0.029± 0.002	0.031 ± 0.012	0.013 ± 0.002	0.013 ± 0.004	>10	0.014 ± 0.008	0.015 ± 0.001
Omi-32	0.010 ± 0.006	0.017 ± 0.000	>10	2.682 ± 0.553	1.018 ± 0.139	0.035 ± 0.016	0.354 ± 0.064	2.341 ± 0.282
Omi-33	0.027 ± 0.011	0.014 ± 0.005	0.042 ± 0.018	0.068 ± 0.022	0.133 ± 0.021	0.013 ± 0.004	0.053 ± 0.006	0.490 ± 0.156
Omi-34	0.007 ± 0.004	0.008 ± 0.001	0.062 ± 0.004	0.009 ± 0.003	0.014 ± 0.000	>10	0.005 ± 0.000	0.020 ± 0.001
Omi-35	0.018 ± 0.004	0.058 ± 0.006	0.381 ± 0.061	0.094 ± 0.004	0.044 ± 0.018	1.687 ± 0.441	0.020 ± 0.000	0.056 ± 0.012
Omi-36 (3-66)	0.022 ± 0.004	0.009 ± 0.003	0.009 ± 0.003	0.030 ± 0.014	0.178 ± 0.048	0.024 ± 0.006	>10	>10
Omi-38	0.015 ± 0.004	0.024 ± 0.015	>10	0.005 ± 0.000	0.008 ± 0.002	0.005 ± 0.001	0.011 ± 0.005	0.010 ± 0.001
Omi-39	0.014 ± 0.002	0.009 ± 0.004	>10	0.026 ± 0.011	0.014 ± 0.001	0.035 ± 0.003	0.027 ± 0.009	0.045 ± 0.017
Omi-41	>10	0.053 ± 0.028	0.037 ± 0.002	>10	0.032 ± 0.007	>10	>10	>10
Omi-42	0.013 ± 0.004	0.007 ± 0.004	0.006 ± 0.002	0.021 ± 0.011	0.025 ± 0.012	0.013 ± 0.001	0.003 ± 0.000	0.007 ± 0.002

(B) IC50 of commercial mAbs against PV BA.2.75 (related to Figure 5B)

	IC50 (μg/mL)						
	Pseudovirus						
	Victoria	BA.1	BA.1.1	BA.2	BA.3	BA.4/5	BA.2.75
REGN10987	0.002 ± 0.001	>10	>10	0.616 ± 0.347	>10	>10	>10
REGN10933	0.001 ± 0.002	>10	>10	>10	>10	>10	>10
AZD1061	0.002 ± 0.001	0.308 ± 0.058	>10	0.008 ± 0.003	0.019 ± 0.007	0.015 ± 0.004	0.021 ± 0.002
AZD8895	0.001 ± 0.000	0.246 ± 0.027	0.100 ± 0.053	1.333 ± 0.317	>10	>10	0.008 ± 0.000
AZD7442	0.001 ± 0.000	0.232 ± 0.113	0.806 ± 0.093	0.008 ± 0.001	0.065 ± 0.011	0.065 ± 0.007	0.017 ± 0.003
ADG10	0.007 ± 0.002	>10	>10	>10	>10	>10	>10
ADG20	0.003 ± 0.002	0.348 ± 0.169	0.253 ± 0.070	>10	>10	>10	>10
ADG30	0.014 ± 0.006	>10	>10	>10	>10	>10	>10
Ly-CoV555	0.002 ± 0.000	>10	>10	>10	>10	>10	>10
Ly-CoV16	0.014 ± 0.010	>10	>10	>10	>10	>10	>10
Ly-CoV1404	0.001 ± 0.000	0.002 ± 0.000	0.001 ± 0.000	0.001 ± 0.000	0.002 ± 0.000	0.002 ± 0.000	0.002 ± 0.000
S309	0.079 ± 0.027	0.113 ± 0.006	0.142 ± 0.012	0.638 ± 0.154	0.311 ± 0.023	0.689 ± 0.041	0.202 ± 0.017

Table S2. **IC50 of BA.1 mAbs against PV BA.2, BA.2.75 and BA.2 with each of the four BA.2.75 mutations (see also Figure S1, related to Figure 5)**

	IC50 (µg/ml)					
mAbs	**BA.2**	**BA.2+D339H**	**BA.2+R493Q**	**BA.2+G446S**	**BA.2.+ N460K**	**BA.2.75**
Omi02	0.003 ± 0.000	0.007 ± 0.003	0.003 ± 0.000	0.007 ± 0.002	0.025 ± 0.003	0.009 ± 0.002
Omi03	0.008 ± 0.001	0.006 ± 0.000	0.002 ± 0.001	0.005 ± 0.001	0.401 ± 0.026	0.017 ± 0.000
Omi06	0.039 ± 0.008	0.012 ± 0.002	0.023 ± 0.010	0.087 ± 0.002	0.026 ± 0.002	0.063 ± 0.005
Omi08	0.114 ± 0.045	0.250 ± 0.009	0.194 ± 0.020	0.017 ± 0.001	0.552 ± 0.090	0.036 ± 0.002
Omi09	0.008 ± 0.002	0.005 ± 0.001	0.003 ± 0.000	0.006 ± 0.001	0.010 ± 0.002	0.003 ± 0.000
Omi12	0.003 ± 0.001	0.003 ± 0.001	0.001 ± 0.000	0.003 ± 0.001	0.011 ± 0.002	0.003 ± 0.001
Omi16	0.034 ± 0.012	0.014 ± 0.004	0.008 ± 0.003	0.018 ± 0.004	>10	>10
Omi17	0.060 ± 0.004	0.036 ± 0.015	0.013 ± 0.001	0.038 ± 0.002	>10	0.255 ± 0.169
Omi18	0.005 ± 0.000	0.003 ± 0.000	0.004 ± 0.000	0.003 ± 0.000	0.014 ± 0.002	0.035 ± 0.007
Omi20	0.015 ± 0.003	0.007 ± 0.000	0.005 ± 0.001	0.005 ± 0.001	0.315 ± 0.142	0.178 ± 0.075
Omi23	0.019 ± 0.005	0.006 ± 0.000	0.007 ± 0.000	0.010 ± 0.002	0.022 ± 0.005	0.011 ± 0.006
Omi24	0.007 ± 0.001	0.005 ± 0.001	0.004 ± 0.000	0.005 ± 0.000	0.014 ± 0.000	0.008 ± 0.004
Omi25	0.024 ± 0.004	0.016 ± 0.003	0.007 ± 0.002	0.022 ± 0.000	0.050 ± 0.010	0.014 ± 0.005
Omi26	0.013 ± 0.001	0.007 ± 0.002	0.008 ± 0.001	0.008 ± 0.002	0.010 ± 0.000	0.010 ± 0.004
Omi27	0.034 ± 0.006	0.007 ± 0.001	0.007 ± 0.001	0.011 ± 0.001	>10	6.672 ± 4.466
Omi28	0.008 ± 0.000	0.009 ± 0.001	0.010 ± 0.001	0.014 ± 0.000	0.103 ± 0.048	0.133 ± 0.082
Omi29	0.056 ± 0.014	0.018 ± 0.006	0.042 ± 0.012	0.024 ± 0.002	>10	>10
Omi30	0.013 ± 0.002	0.006 ± 0.001	0.002 ± 0.000	0.003 ± 0.000	0.018 ± 0.001	0.008 ± 0.002
Omi31	0.011 ± 0.002	0.005 ± 0.001	0.003 ± 0.000	0.005 ± 0.001	0.015 ± 0.001	0.014 ± 0.008
Omi32	2.614 ± 0.533	0.683 ± 0.179	0.312 ± 0.008	0.330 ± 0.010	2.341 ± 0.282	0.354 ± 0.064
Omi33	0.070 ± 0.024	0.177 ± 0.035	0.063 ± 0.008	0.043 ± 0.016	0.490 ± 0.156	0.053 ± 0.006
Omi34	0.009 ± 0.003	0.004 ± 0.000	0.002 ± 0.000	0.002 ± 0.000	0.020 ± 0.001	0.005 ± 0.000
Omi35	0.092 ± 0.004	0.012 ± 0.003	0.017 ± 0.011	0.014 ± 0.006	0.056 ± 0.012	0.020 ± 0.000
Omi36	0.030 ± 0.014	0.036 ± 0.002	0.013 ± 0.003	0.067 ± 0.015	>10	>10
Omi38	0.005 ± 0.000	0.011 ± 0.000	0.003 ± 0.001	0.010 ± 0.000	0.010 ± 0.001	0.011 ± 0.005
Omi39	0.026 ± 0.011	0.012 ± 0.002	0.021 ± 0.007	0.009 ± 0.002	0.045 ± 0.017	0.027 ± 0.009
Omi41	>10	>10	>10	>10	>10	>10
Omi42	0.021 ± 0.011	0.011 ± 0.002	0.006 ± 0.001	0.016 ± 0.002	0.007 ± 0.002	0.003 ± 0.000

	BA.1 infection	BA.2 infection	BA.4/5 infection	AZV3+28	BNT162b2 V3+28	Early pandemic	Alpha	Beta	Gamma	Delta	Vaccine-V1_Delta	Delta-V1-Vaccine
Participants												
Female	7	7	7	7	7	7	7	7	7	7	7	7
Male	7	4	5	21	10	9	6	5	4	3	4	4
Median Age (Y)	22 (Range 21-56)	41 (Range 22-57)	42 (Range 20-94)	37 (Range 25-53)	45 (Range 30-59)	60 (Range 53-69)	57 (Range 29-76)	47 (Range 16-64)	32 (Range 23-49)	26 (Range 12-36)	40 (Range 28-70)	41 (Range 31-54)

Table S3. Sample participant information.

Table S4. **Primers used for site-directed PCR mutagenesis to generate the BA.2.75 construct using the BA.2 Spike construct as template (related to methods)**

Primer ID	Sequence
D339H_pNeoF	5′-GGTTGCGTAGCTGAAACCGGTACCAATCTGTGCCCTTTCCACGAGGTGTTCAATGCCACC-3′
G446S_F	5′-CAAACTAGATTCGAAAGTTAGCGGCAATTACAATTACCTG-3′
G446S_R	5′-CAGGTAATTGTAATTGCCGCTAACTTTCGAATCTAGTTTG-3′
N460K_F	5′-CAGACTGTTCAGAAAGAGCAAACTGAAGCCTTTCGAGAGAGAC-3′
N460K_R	5′-GTCTCTCTCGAAAGGCTTCAGTTTGCTCTTTCTGAACAGTCTG-3′
R493Q_F (RBD)	5′-CAATTGCTACTTCCCTCTGCAGAGCTACGGCTTCAGACCTACC-3′
R493Q_R (RBD)	5′-GGTAGGTCTGAAGCCGTAGCTCTGCAGAGGGAAGTAGCAATTG-3′
RBD333_BAP_R	5′-GTCATTCAGCAAGCTCTTCTTGCCGCACACGGTAGC-3′
pNeoRBD333Omi_F	5′-GGTTGCGTAGCTGAAACCGGTCATCACCATCACCATCACACCAATCTGTGCCCTTTCGAC-3′
K147E_W152R_F157L_F	5′-CGTTTATTATCATGAGAACAACAAGAGCAGGATGGAGAGCGAGTTACGCGTATATTCGTCGGC-3′
K147E_W152R_F157L_R	5′-GCCGACGAATATACGCGTAACTCGCTCTCCATCCTGCTCTTGTTGTTCTCATGATAATAAACG-3′
I210L_F	5′-CAGCAAGCACACACCCGTTAATCTGGGCAGAGACC-3′
I210L_R	5′-GGTCTCTGCCCAGATTAACGGGTGTGTGCTTGCTG-3′
G275S_F	5′-GCGATTCGTCAAGCAGTTGGACCGCTGGAGC-3′
G275S_R	5′-GCTCCAGCGGTCCAACTGCTTGACGAATCGC-3′
D339H_F	5′-CAATCTGTGCCCTTTCCACGAGGTGTTCAATGC-3′
D339H_R	5′-GCATTGAACACCTCGTGGAAAGGGCACAGATTG-3′
G446S_N460K_F	5′-GAACTCTAACAAACTAGATTCGAAAGTTAGCGGCAATTACAATTACCTGTACAGACTGTTCAGAAAGAGCAAGCTGAAGCCTTTCGAGAG-3′
G446S_N460K_R	5′-CTCTCGAAAGGCTTCAGCTTGCTCTTTCTGAACAGTCTGTACAGGTAATTGTAATTGCCGCTAACTTTCGAATCTAGTTTGTTAGAGTTC-3′
R493Q_F	5′-GCTTCAATTGCTACTTCCCTCTGCAGAGCTACGGCTTCAGACCTACC-3′
R493Q_R	5′-GGTAGGTCTGAAGCCGTAGCTCTGCAGAGGGAAGTAGCAATTGAAGC-3′

Table S5. X-ray data collection and structure refinement statistics (related to Figure 4)

[a] Values in parentheses are for highest-resolution shell.

Structure	BA.2.75 RBD/ACE2
PDB ID	8ASY
Data collection	
Space group	$P4_12_12$
Cell dimensions	
a, b, c (Å)	105.3, 105.3, 220.8
a, b, g (°)	90, 90, 90
Resolution (Å)	76–2.85 (2.80–2.85)[a]
R_{merge}	0.443 (---)
R_{pim}	0.086 (1.401)
I/s(I)	7.6 (0.4)
$CC_{1/2}$	0.971 (0.279)
Completeness (%)	99.8 (96.9)
Redundancy	26.8 (25.7)
Refinement	
Resolution (Å)	76–2.85
No. reflections	2089/1439
R_{work} / R_{free}	0.217/0.265
No. atoms	
Protein	6464
Ligand/ion/water	167
B factors (Å^2)	
Protein	86
Ligand/ion/water	108
r.m.s. deviations	
Bond lengths (Å)	0.002
Bond angles (°)	0.4